The Journal of Immunology

The Scaffolding Protein IQGAP1 Interacts with NLRC3 and Inhibits Type I IFN Production

Aaron M. Tocker, Emily Durocher, Kimberly D. Jacob, Kate E. Trieschman, Suzanna M. Talento, Alma A. Rechnitzer, David M. Roberts and Beckley K. Davis

J Immunol 2017; 199:2896-2909; Prepublished online 1 September 2017;
doi: 10.4049/jimmunol.1601370
http://www.jimmunol.org/content/199/8/2896

The Journal of Immunology is published twice each month by
The American Association of Immunologists, Inc.,
1451 Rockville Pike, Suite 650, Rockville, MD 20852

Print ISSN: 0022-1767 Online ISSN: 1550-6606.

The Scaffolding Protein IQGAP1 Interacts with NLRC3 and Inhibits Type I IFN Production

Aaron M. Tocker,[1] Emily Durocher,[1] Kimberly D. Jacob,[1] Kate E. Trieschman, Suzanna M. Talento, Alma A. Rechnitzer, David M. Roberts, and Beckley K. Davis

Sensing of cytosolic nucleotides is a critical initial step in the elaboration of type I IFN. One of several upstream receptors, cyclic GMP–AMP synthase, binds to cytosolic DNA and generates dicyclic nucleotides that act as secondary messengers. These secondary messengers bind directly to stimulator of IFN genes (STING). STING recruits TNFR-associated NF-κB kinase–binding kinase 1 which acts as a critical node that allows for efficient activation of IFN regulatory factors to drive the antiviral transcriptome. NLRC3 is a recently characterized nucleotide-binding domain, leucine-rich repeat containing protein (NLR) that negatively regulates the type I IFN pathway by inhibiting subcellular redistribution and effective signaling of STING, thus blunting the transcription of type I IFNs. NLRC3 is predominantly expressed in lymphoid and myeloid cells. IQGAP1 was identified as a putative interacting partner of NLRC3 through yeast two-hybrid screening. In this article, we show that IQGAP1 associates with NLRC3 and can disrupt the NLRC3–STING interaction in the cytosol of human epithelial cells. Furthermore, knockdown of IQGAP1 in THP1 and HeLa cells causes significantly more IFN-β production in response to cytosolic nucleic acids. This result phenocopies NLRC3-deficient macrophages and fibroblasts and short hairpin RNA knockdown of NLRC3 in THP1 cells. Our findings suggest that IQGAP1 is a novel regulator of type I IFN production, possibly via interacting with NLRC3 in human monocytic and epithelial cells. ***The Journal of Immunology*****, 2017, 199: 2896–2909.**

The vertebrate innate immune system is characterized by germline-encoded pattern recognition receptors (PRRs) that can directly bind to or indirectly sense pathogen-associated molecular patterns (PAMPs). The activation of PRRs by their cognate PAMPs initiates several diverse signaling cascades such as the NF-κB, MAPK, and IFN regulatory factors (IRFs). These pathways lead to robust cytokine or IFN secretion that is specific for the type of pathogen. Most PRRs have been grouped into five superfamilies based on amino acid sequence homology and domain organization. These families include the TLRs, C-type lectin receptors, RIG-I–like receptors, AIM2-like receptors, and the nucleotide oligomerization domain (NOD)–like receptors or nucleotide-binding domain (NBD), leucine-rich repeat (LRR) containing proteins (NLRs) (1). Individual PRRs occupy many distinct extra- and intracellular locations. Several PRRs and their signaling molecules have been shown to dynamically redistribute within the cell to more efficiently effect their function, which ultimately leads to a rapid immune response (2).

The secretion of type I IFN is a critical step in the initiation of the immune response to cytosolic DNA, RNA, and nucleotide metabolites. The mechanisms of type I IFN production have been studied extensively (3). Recent evidence has identified key signaling molecules and both positive and negative regulators of this pathway. There is a manifold array of cytosolic sensors of nucleic acids that induce type I IFN in response to viral and bacterial infections. For example, cyclic GMP–AMP (cGAMP) synthase (cGAS) binds directly to dsDNA in the cytosol in a sequence-independent manner by interacting with the sugar phosphate backbone of DNA. Therefore, cGAS can bind dsDNA from multiple sources such as DNA viruses (HSV), eukaryotic nuclear DNA (calf thymus), and prokaryotic DNA (bacteria) insofar as they are located in the host cytosol. Binding of dsDNA, ATP, and GTP to cGAS causes dimerization and dramatic conformational changes, opening the active site of cGAS to generate cGAMP, which is a type of cyclic dinucleotide (CDN) that can act as a secondary messenger (4–6). CDNs bind directly to the ER transmembrane protein stimulator of IFN genes (STING) (also known as MITA, MYPY, ERIS, and TMEM173), causing its dimerization (7–11). The STING dimers can interact with and activate TNFR-associated NF-κB kinase (TANK)–binding kinase (TBK1) at the mitochondrial-associated ER membranes (MAMs). Active TBK1

Department of Biology, Franklin and Marshall College, Lancaster, PA 17604

[1]A.M.T., E.D., and K.D.J. contributed equally to this work.

ORCIDs: 0000-0002-9672-0357 (A.M.T.); 0000-0001-9777-1781 (E.D.); 0000-0001-7158-7935 (S.M.T.); 0000-0003-0673-8017 (B.K.D.).

Received for publication August 8, 2016. Accepted for publication August 7, 2017.

This work was supported by National Institutes of Health Grant R15 DK098754 (to B.K.D.), startup funds from Franklin and Marshall College (to B.K.D.), and an Undergraduate Science Education Award from the Howard Hughes Medical Institute to Franklin and Marshall College (52007538). This material is based upon work supported by the National Science Foundation under Grant 1626073.

The content is solely the responsibility of the authors and does not necessarily represent the official views of the National Institutes of Health or the National Science Foundation.

Address correspondence and reprint requests to Dr. Beckley K. Davis, Franklin and Marshall College, PO Box 3003, Lancaster, PA 17604-3003. E-mail address: beckley.davis@fandm.edu

The online version of this article contains supplemental material.

Abbreviations used in this article: BIR, baculovirus IAP repeat; CARD, caspase recruitment domain; CDN, cyclic dinucleotide; cGAMP, cyclic GMP–AMP; cGAS, cGAMP synthase; Clasp2, cytoplasmic linker–associated protein 2; C2TA, MHC class 2 transactivator; Dia1, diaphanous-related formin; ER, endoplasmic reticulum; HA, hemagglutinin; IRF, IFN regulatory factor; ISG, IFN-stimulated gene; LRR, leucine-rich repeat; MAM, mitochondrial-associated ER membrane; MAVS, mitochondria antiviral signaling; NACHT domain, NAIP, C2TA, HET-E, and TP1 domain; NAIP, neuronal apoptosis inhibitor protein; NBD, nucleotide-binding domain; NLR, NBD, LRR-containing protein; NNBD, CARD with NBD; NOD, nucleotide oligomerization domain; PAMP, pathogen-associated molecular pattern; PRR, pattern recognition receptor; PYD, pyrin domain; QPCR, quantitative PCR; RGCT, RasGAP C-terminal; RNF5, RING-finger protein 5; SEAP, secreted embryonic alkaline phosphatase; shRNA, short hairpin RNA; STING, stimulator of IFN genes; TANK, TNFR-associated NF-κB kinase; TBK1, TANK binding kinase 1; TP1, telomerase-associated protein; ULK1, UNC-51–like kinase; WHD, winged helix domain.

can phosphorylate IRF3 and IRF7 to promote dimerization and nuclear translocation. Nuclear IRFs in combination with NF-κB subunits activate IFN-stimulated gene (ISG) transcription (12). Intracellular bacterial pathogens such as *Listeria monocytogenes* and *Microbacteria tuberculosis* generate unique CDNs (cyclic di-AMP and GMP) as metabolic byproducts bypassing the requirement for cGAS activity (13–16). Both host- and pathogen-derived CDNs bind directly to STING, inducing different conformational changes that ultimately lead to IRF3/7 activation (7).

Both host and pathogen can negatively regulate the inflammatory response to CDNs. STING dynamically relocalizes from the ER via the Golgi apparatus to cytosolic vesicles, possibly via an atypical autophagy response. The redistribution of STING is mediated by several autophagy-mediated signaling proteins, ULK1/ATG1 and ATG9, to possibly act as a brake on type I IFN production (17, 18). In the absence of *Atg9*, STING is targeted for proteosomal degradation via endogenous RING-finger protein 5 (RNF5)–dependent ubiquitination (19). Additionally, HSV has been shown to encode several open reading frames that inhibit STING-dependent *IFNb* production. For example, vIRF1 can inhibit TBK1 binding to STING and prevent IRF3 phosphorylation; additionally, vIRF1 has been shown to inhibit p300 histone acetylation which blocks IRF3 recruitment of histone-modifying enzymes (20). Many other pathogen-escape pathways have been described which suggest that targeted inhibition of type I IFN provides a selective advantage for the pathogen (21).

It is important to note that there is growing evidence that NLR proteins are pleiotropic and can act in many pathways. Several NLRs have been shown to bind directly to PAMPs and act as bona fide PRRs (22–24). Others appear to have regulatory roles that indirectly influence pathogen sensing or the regulation of inflammation. However, there is evidence that supports the model that NLR proteins respond cooperatively or redundantly to the same pathogen, or that single NLRs can regulate disparate pathways which may be cell or species specific (25). For example, recent evidence has suggested that NLRC3 can also act as a negative regulator of the PI3K–mTOR pathway in epithelial cells, which is involved in colorectal carcinogenesis (26), as well as affecting the type I IFN and proinflammatory pathways. Likewise, NLRX1 has been shown to be involved in negatively regulating multiple tumorigenic pathways (27–29) as well as other inflammatory pathways (23, 28, 30–32). These recent advances in the field have challenged the model that single NLR proteins are pathogen or pathway specific. NLR proteins are characterized by a central NOD which is comprised of a NACHT domain (neuronal apoptosis inhibitor protein [NAIP], MHC class 2 transactivator [C2TA], HET-E [incompatibility locus protein from *Podospora anserina*], and telomerase-associated protein [TP1]) or NBD, two helical domains (HD1 and HD2), and a winged helix domain (WHD); preceded by an N terminus effector domain (either a caspase recruitment domain [CARD]), pyrin domain [PYD], baculovirus IAP repeat [BIR], or undefined domains) and a series of variable LRRs at the C terminus (25). Several NLRs have been shown to assemble into large macromolecular complexes: inflammasomes (NLRP1, NLRP3, NLRC4/NAIP, and others), enhanceosomes (CIITA, NLRC5, and possibly NLRP3; Ref. 33), NODosomes (NOD1 and NOD2), and a TRAFasome (NLRC3) (34, 35). The formation of these complexes is mediated by the scaffolding ability of individual NLRs to recruit diverse sets of interacting proteins. These protein–protein interactions can be mediated by each of the three domains of NLRs facilitating the recruitment of multiple binding partners, possibly in series or in tandem.

NOD2 (36–41), NLRX1 (42–46) NLRP4 (47), and NLRC3 (48) have been implicated in sensing viral infections in vitro and in vivo. However, the mechanisms are poorly understood and debated within the field (49, 50). Future studies will be needed to address the precise roles of individual NLR proteins in response to viral pathogens. These studies will help further define the cell type–, pathogen-, and spatiotemporal-specific responses. NLRC3 is a poorly characterized NLR that negatively regulates several pathways in many different cell types. NLRC3 contains an N-terminal CARD-like region, a central NBD, and a series of multiple LRRs. The Ting laboratory has shown that NLRC3 can act as a negative regulator of several signaling pathways in T lymphocytes (51), macrophages (52), and epithelial/fibroblast cells (48). NLRC3 was shown to interact with TRAF6 via a TRAF2-consensus binding site in human myeloid and epithelial cells. In mice, this interaction inhibited the NF-κB–dependent signaling during experimental colitis induced by cecal ligation puncture (52). In a different system it was shown that recombinant purified NLRC3 binds directly to STING, and NLRC3 coimmunoprecipitates both STING and TBK1. In HeLa cells this interaction inhibited the redistribution of STING to the perinuclear region and blunted the TBK1-dependent phosphorylation of IRF3. In vivo NLRC3 was necessary for limiting type I IFN in response to lethal HSV infection. *Nlrc3*$^{-/-}$ mice infected with HSV showed decreased morbidity and enhanced innate immunity (48). These data suggest that NLRC3 is a negative regulator of virus-induced IFN responses.

Because of the diverse nature of the inhibitory ability of NLRC3, we sought to identify novel protein–protein interaction pathways associated with NLRC3 by yeast two-hybrid screening. These screens yielded several candidate proteins. In this article, we show that IQGAP1, a scaffolding protein involved in diverse cellular processes, specifically interacts with NLRC3 and can disrupt the NLRC3–STING interaction. IQGAP1 is a highly conserved protein that has multiple protein–protein interaction domains. The role of IQGAP1 in the immune system is not well understood, but it may function to distribute signaling molecules to specific subcellular regions within the cell or facilitate the coordination of positive and negative regulators (53). In human transformed cells, IQGAP1 has been shown to negatively regulate cytokine secretion in response to TCR ligation in Jurkat T cells (54) by negatively regulating F-actin at the immunological synapse, whereas it positively regulates degranulation of NK-like cells (55) by controlling the microtubule organizing center. Additionally, IQGAP1 has been shown to be involved in IL-1β secretion in bone marrow–derived macrophages in response to *Yersinia pestis* (56). *IQGAP1* and *NLRC3* are expressed in hematopoietic and nonhematopoeitic tissues and partially colocalize in the cytosol/cytoplasm within epithelial cells. IQGAP1 shRNA-mediated knockdown in THP1 and HeLa cells phenocopy NLRC3 in response to cytosolic DNA stimulation, implying that the NLRC3–IQGAP1 complex inhibits cGAS-dependent cytosolic DNA sensing. We show that NLRC3 specifically interacts with IQGAP1 and this interaction can inhibit the NLRC3–STING interaction. These data support the hypothesis that the NLRC3–IQGAP1 complex may act as a negative regulator of type 1 IFN, inhibiting the cells' ability to mount a hyper-IFN response, possibly acting as a biological rheostat. To our knowledge, these data are the first to illustrate a role for IQGAP1 in the type 1 IFN signaling pathway.

Materials and Methods

Cell culture and transfections

Human embryonic kidney (HEK293T), SW480, and HeLa cells were maintained in DMEM (Sigma) supplemented with 10% FBS (Invitrogen), 20 U penicillin, 20 mg streptomycin, 1× sodium pyruvate (Life Technologies), and 146 mg of L-glutamine mixture (Life Technologies). THP1 and THP1-Dual Cells (InvivoGen) were grown in RPMI 1640 (Life

Technologies) supplemented as described above. All cells were grown at 37°C and 5% CO_2.

HEK293T, SW480, and HeLa cells were seeded into six-well plates at a density of between 1 and 5 × 10^5 cells per well and transfected with epitope-tagged constructs using Lipofectamine 2000 (Invitrogen) at a ratio of 3:1 according to the manufacturer's protocol. Cells were processed 18–24 h after transfection.

Stable knockdown in human cell lines

HeLa, THP1, and THP1-Dual Cells were transduced with shRNA lentiviral particles produced from plasmid DNA for human shRNA for IQGAP1 (Mission TRCN0000298928, TRCN0000298930, TRCN0000298931; Sigma-Aldrich) according to the manufacturer's protocol. The *IQGAP1* shRNA-transduced clones were selected with 0.6 μg/ml puromycin. To determine efficiency of knockdown, RNA was isolated from cells using Trizol Reagent (Life Technologies), following the manufacturer's protocol, and mRNA levels were assessed by RT-PCR (data not shown). IQGAP1 protein expression levels were evaluated by immunoblotting with rabbit anti-IQGAP1 (1:5000; Abcam) Ab.

Coimmunoprecipitations, subcellular fractionation, and Western blotting

Cells were lysed in 1× PBS, 1% Triton X-100, and 0.05% sodium deoxycholate supplemented with protease inhibitor mixture for 30 min at 4°C. The lysates were then cleared by centrifugation (14,000 × *g*, 15 min at 4°C), incubated with mouse anti-Flag M2 Ab (1:1000; Sigma) for 4 h at 4°C, and immunoprecipitated using Protein A/G Ultralink Resin (Pierce) for 24 h while shaking at 4°C. Immunoprecipitates were washed three times in PBS and 1% Triton X-100 and 0.05% deoxycholate. Samples were analyzed using SDS-PAGE (using 4–15% Mini-PROTEAN TGX Gels). Gels were then transferred to nitrocellulose membrane (Bio-Rad). Immunoblots were probed with anti-Flag M2 conjugated to HRP (1:5000; Sigma), anti-hemagglutinin (HA) conjugated to HRP (1:5000; Sigma), rabbit anti-GFP (1:5000; Sigma), and goat anti-rabbit IgG HRP (1:5000; Santa Cruz). Transfected SW480 cells were fractionated using a subcellular fractionation kit for cultured cells (Pierce) per the manufacturer's suggested protocol. Rabbit mAbs to PKM2, vimentin, CoxIV, and H3 (1:1000; Cell Signaling) were used to probe immunoblots of subcellular fractions.

Immunofluorescence

SW480 and HeLa cells were seeded in a six-well dish containing glass coverslips at a density of 5 × 10^5 cells per well and transfected as previously described. After 24 h, the cells were fixed using 4% formaldehyde (Sigma-Aldrich) in 1× PBS for 10 min, then washed three times with 1× PBS, and blocked with PBTN (1× PBS, 1% normal goat serum, and 0.1% Triton X-100) for 15 min. Cells were then stained with mouse anti-Flag M2 (1:1000; Sigma) or rat anti-Flag (1:1000; Novus), rat anti-HA (1:1000; Roche), chicken anti-HA (1:1000; Abcam), mouse anti-HA (1:1000; Sigma-Aldrich) or rabbit anti-HA (1:1000; Cell Signaling), and rabbit anti-V5 (1:1000; Cell Signaling) or mouse anti-V5 (1:1000; Life Technologies). We observed no differences in staining between different species and/or isotypes of Abs used in our studies (data not shown). Primary Abs to HSP60, NUP98, and PKM2 were purchased from Cell Signaling Technologies (1:300). Phalloidin conjugated to either Alexa Fluor 488, 568, or 647 was used (1:1000; Life Technologies). Rabbit anti-Tomm20 (1:1000; Abcam) was used to identify mitochondria. Species- and isotype-matched goat secondary Abs conjugated to various Alexa Fluor dyes were used (1:5000; Life Technologies) with DAPI nuclear counterstain. Cells were imaged using a Nikon E400 epifluorescent microscope with a camera, a Leica SP8 confocal microscope equipped with five laser lines, or with a white-light laser at Franklin and Marshall College or the Imaging Core at Pennsylvania State College of Medicine, respectively.

Secreted embryonic alkaline phosphatase/Luciferase reporter analysis and ELISA

THP1-Dual Cells were seeded into 12-well plates at a density of 5 × 10^5 cells per well and transfected with 5 μg/ml 2′2′ or 3′3′ cGAMP and 1 μg/ml immunostimulatory DNA or HSV DNA (InvivoGen) with Lipofectamine 3000 per the manufacturer's suggested protocol. Secreted embryonic alkaline phosphatase (SEAP) and Lucia activity were measured 24 h after induction using QUANTI-Blue (InvivoGen) and QUANTI-Luc (InvivoGen) according to the manufacturer's protocol. Tissue culture supernatants from stimulated cells were assayed for TNF-α, IL-1β (BD Biosciences), and IFN-β (Antigenix) by sandwich ELISA using the manufacturers' suggested protocols.

Vector construction

The full-length IQGAP1 open reading frame was amplified from a plasmid template using a mixture of Platinum Pfx and Taq polymerases (Life Technologies) and cloned into the pCR8/TOPO/TA (Life Technologies) base vector by TOPO TA cloning. The truncations of IQGAP1 and NLRC3 were amplified from full-length template using the primers listed in Table I (Integrated DNA Technologies) and cloned into the pCR8/TOPO/TA (Life Technologies) base vector. Recombination reactions were performed into modified FLAG or fluorescent protein gateway destination vectors (described in Ref. 57) using LR Clonase II (Life Technologies). Generation of the NLRC3 plasmid has been previously described (51). ColorfulCell was a gift from P. Neveu (plasmid number 62449; Addgene); pEGFP-IQGAP1 was a gift from D. Sacks (plasmid number 30112; Addgene); pCAG-mGFP was a gift from C. Cepko (plasmid number 14757; Addgene); and epitope-tagged mitochondria antiviral signaling (MAVS) (also known as VISA, IPS1, and CARDIF), human STING, and human TBK1 were provided by J. Ting from the University of Chapel Hill. STING was subcloned into pCDNA3.1D to provide a C-terminal V5 tag. All vector sequences were verified by bidirectional sequencing.

Yeast two-hybrid screening

A yeast two-hybrid screen was completed by Hybrigenics (Paris, France) using a truncation of human NLRC3 consisting of amino acids 1–600 as the bait and a human leukocyte and activated mononuclear cell cDNA library as the prey. Additionally, two small-scale library screens were performed in our laboratory using MAV203 cells (Life Technologies). These screens used full-length human NLRC3 as the bait and a normalized human universal library (Dual Systems) as the prey. In brief, 10 μg of both bait and prey DNA was added to 250 μl of MAV203 cells in duplicate. To each tube a polyethylene glycol/lithium acetate solution was added and tubes were incubated for 30 min in a 30°C water bath. After the addition of sterile DMSO, the cells were heat shocked at 42°C for 20 min, pelleted, and resuspended in sterile PBS. Four hundred microliters of cells were plated onto -Leu/-Trp/-His/-Ura plates and incubated at 30°C. The resulting colonies were picked, placed into 100 μl LiOAc plus 1% SDS, and heated at 70°C for 5 min. Following the addition of 300 μl 70% ethanol, the cells were pelleted at 15,000 × *g* for 3 min and washed with 70% ethanol. The pellets were resuspended into 100 μl sterile water and spun at 15000 × *g* for 15 s to pellet debris. PCR was then performed using Dream TAQ DNA polymerase (Thermo Scientific) and 1 μl of the supernatant of the resuspended pellet. Bidirectional sequencing was performed using 5 μl of the PCR product to identify the interactors of human NLRC3.

RT- and quantitative PCR, bar coding, and microarray database searches

Human Multiple Tissue cDNA Panels I and II (Clontech) were used as templates to determine expression patterns of *NLRC3* and *IQGAP1*. Briefly, 1–2 μl of cDNA was amplified using Phusion 2× master mix. The cycling conditions were as follows: 94°C for 10 s, 55°C for 15 s, and 72°C for 30 s for 25 cycles (*GAPDH*), 30 cycles (*IQGAP1*) or 33 cycles (*NLRC3*). Total RNA was harvested from Jurkat, THP1, HeLa, and HEK293T cells using Trizol reagent (Life Technologies), treated with DNAse I (Sigma-Aldrich), and reverse transcribed using RevertAid Reverse Transcriptase (Life Technologies). Quantitative PCR (QPCR) was performed with primers for *NLRC3* and *HPRT* using AmpliTaq (Applied Biosystems) on a Bio-Rad CFX96 machine. Values were calculated by relative expression to *HPRT* using the Δ cycle threshold method. The NextBio (https://www.nextbio.com/) database was searched for IQGAP and NLRC3. Raw data were downloaded and specific cell types were graphed. Molecular bar codes were obtained from The Gene Expression 3.0 program (http://barcode.luhs.org) using the "probe set pages" option. The HGU133plus2 (human) version 3 platform was used and the tissue graph was selected to show only immune cells and tissues from Affymetrix arrays. The affinity probe sets examined were IQGAP1 (200791_s_at) and NLRC3 (236295_s_at). The resulting graphs showing Z-scores ± median absolute deviation were used.

Statistical analysis

Two-way ANOVA with Tukey post hoc statistical analyses were done using Prism 5.0 for Macintosh. Data are represented as mean ± SD of triplicates. Significance is represented by $*p < 0.05$.

Results

Yeast two- hybrid screen

To investigate putative protein interactions with NLRC3, we performed yeast two-hybrid screens. A C-terminal truncation (amino acids 1–600, containing the CARD and a majority of the NBD) and full-length NLRC3 were used to screen a human-activated peripheral mononuclear cell cDNA library and a universal human cDNA library, respectively. We initially performed a yeast two-hybrid screen with a bait construct lacking the LRR because the LRR is a potential autoinhibiting structure that might mask potential interacting partners. Recent crystal structures and functional studies of mouse Nlrc4 and rabbit NOD2 support the hypothesis that the LRRs maintain NLRs in a closed or inhibited confirmation, possibly to prevent premature activation (58, 59). Based on molecular modeling of NLRC3 on rabbit NOD2 (data not shown), the truncation construct used for our screens should contain the known structural domains (see Fig. 1A) that correspond to a functional NOD. However, the crystal structure for NLRC3 has not been published and the exact three-dimensional conformation of the NOD is unknown. In our studies, two separate libraries were used. First, to enrich for immune system–specific interactions, we screened a human leukocyte and activated mononuclear cell library. Additionally, we screened a human universal cDNA library to potentially uncover nonhematopoietic interacting proteins. Over 10^7 clones were screened. Seven clones from the independent screens identified the C terminus of IQGAP1 as a putative interacting region, strongly suggesting that this interaction may occur in multiple cell types. Fig. 1A depicts the bait-and-prey constructs from our screens. IQGAP1 is a well-characterized scaffold protein involved in many disparate cellular responses. Sequence analysis of yeast colonies revealed that the RasGAP C-terminal (RGCT) domain of IQGAP1 interacts with the CARD with NBD (NNBD) region of NLRC3. The RGCT domain is highly conserved (>91% identity and 95% similarity) in vertebrate evolution (Fig. 1B). Likewise, the NBD region of NLRC3 is well conserved (77% identity and 84% similarity) between humans and mice (51).

Expression profiling of IQGAP1 and NLRC3

Previous data have shown that *NLRC3* is expressed in human innate and adaptive immune cells. *NLRC3* was most abundantly expressed in Jurkat T cells, with modest expression in Raji B cells, HL-60, and THP1 monocytic cells. Bioinformatic mining of the Human Protein Atlas supported these findings (51). The initial characterization of *IQGAP1* demonstrated that it was expressed in many different tissues, with the exception of brain (60). Additionally, it has been shown that *IQGAP1* is expressed in many tumors and transformed cells lines including Jurkat T cells (54) and HL-60 cells (61). We have also verified that IQGAP1 is expressed in THP1 and HeLa cells (Supplemental Fig. 1). To confirm and extend the initial expression profiling of both *NLRC3* and *IQGAP1* we used endpoint RT-PCR on commercially available human cDNA panels. We chose to focus on human cells, cell lines, and tissues. The results are shown in Fig. 2A. *IQGAP1* has a broad tissue-expression profile, but was not expressed in the brain

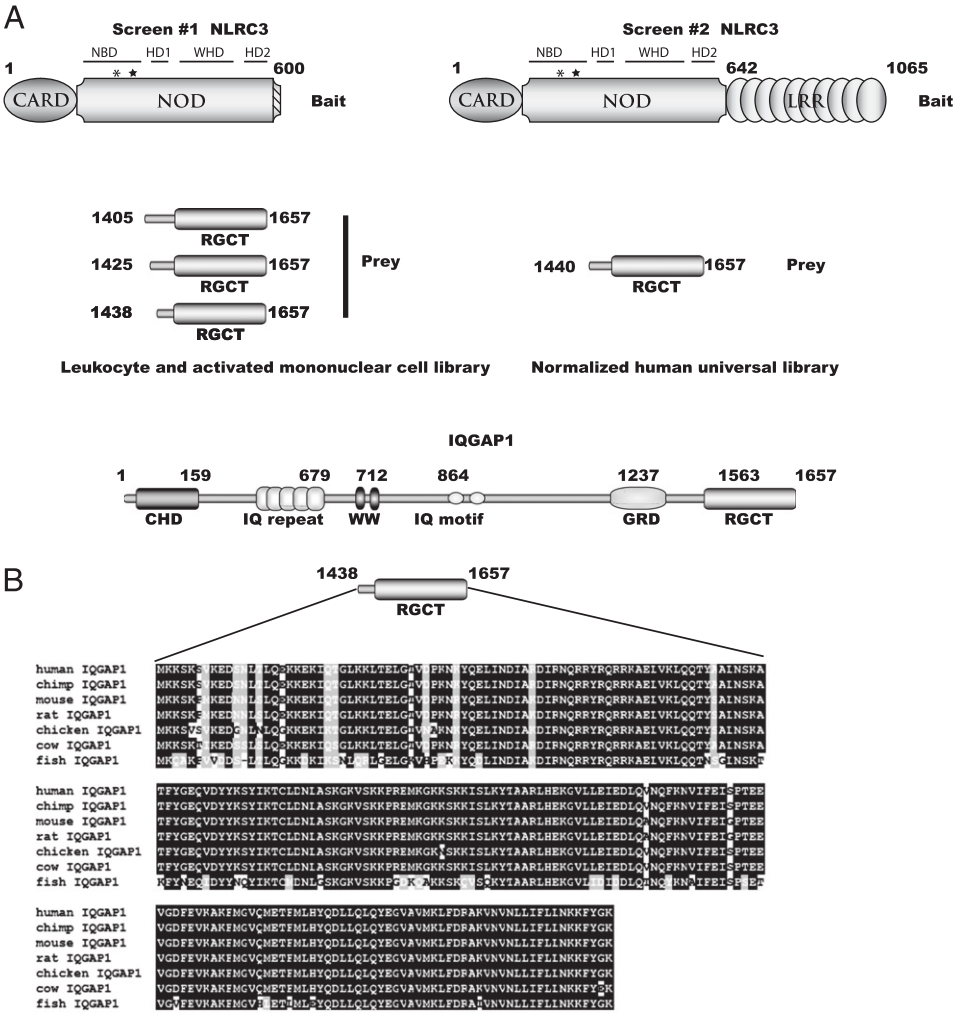

FIGURE 1. NLRC3 yeast two-hybrid constructs. (**A**) Schematic representation of both bait (NLRC3) and prey (IQGAP1) constructs used to screen with a human leukocyte and activated mononuclear cell or human universal cDNA libraries. The * and ★ represent the approximate locations of the Walker A and Walker B motifs. (**B**) Amino acid alignment represents the minimal binding region of IQGAP1, amino acids 1438–1657. CHD, calponin homology domain; GRD, rasGAP-related domain; HD1, helical domain 1; HD2, helical domain 2.

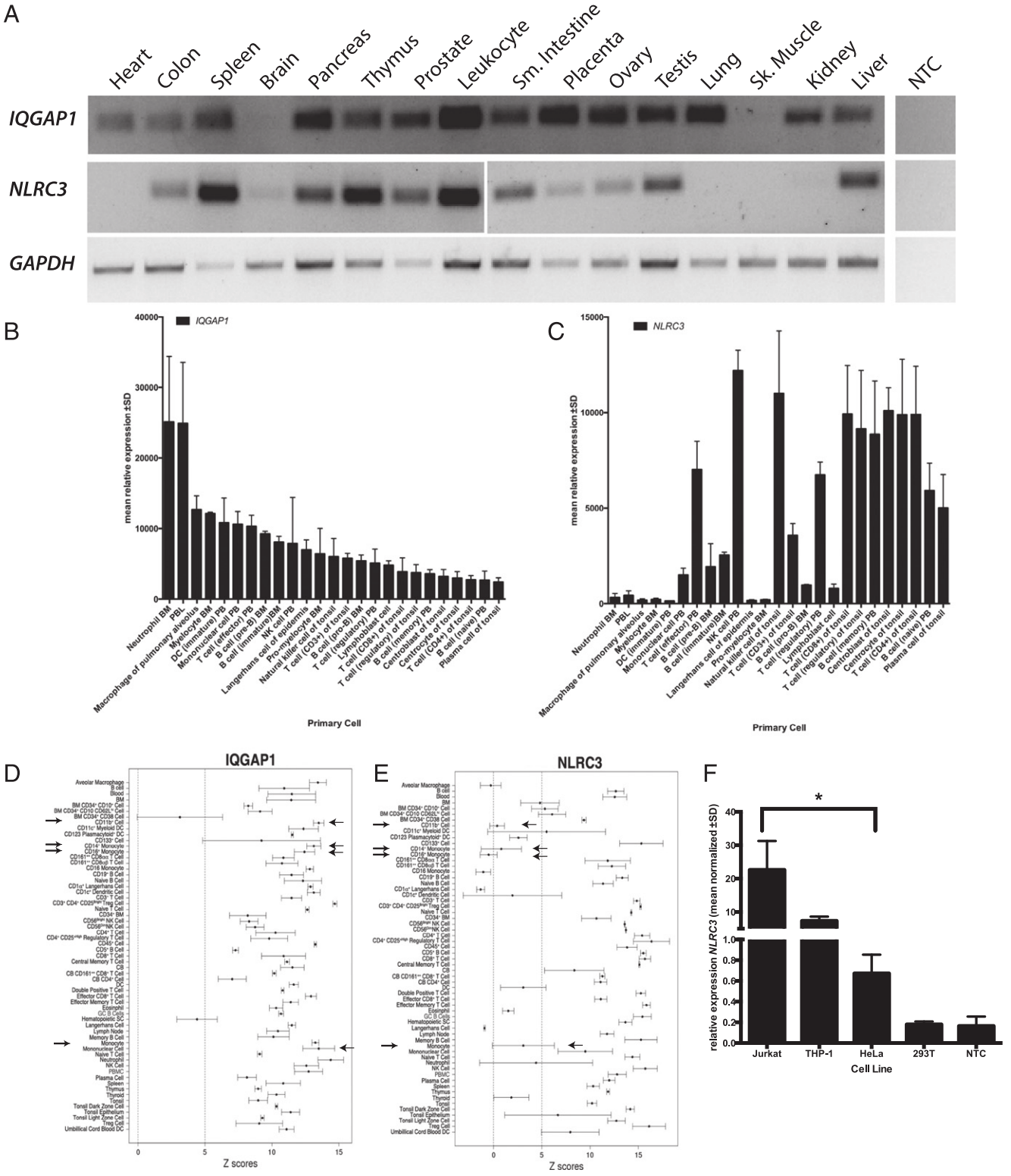

FIGURE 2. *IQGAP1* and *NLRC3* are preferentially expressed in the immune system. (**A**) RT-PCR was used to determine the tissue expression of human *IQGAP1* and *NLRC3*. GAPDH was used as a positive control. BioGPS was queried for human *IQGAP1* and *NLRC3* expression in specific immune cells. The top overlapping cells and tissues for IQGAP1 and NLRC3 were graphed. (**B**) Microarray results show relative *IQGAP1* expression is highest in myeloid cells with moderate levels in lymphocytes. (**C**) Relative *NLRC3* expression is highest in lymphocytes with moderate expression in myeloid cells. (**D** and **E**) Across-tissue expression for *IQGAP1* (probe 200791_s_at) and *NLRC3* (probe 236295_s_at), using immune cells and tissues, are shown. Z-scores ± median absolute deviation is plotted. A dashed line represents a Z-score of 5 which signifies that a given transcript is expressed in a tissue. Arrows depict cells of monocyte/macrophage lineage. (**F**) QPCR analysis of *NLRC3* expression in human transformed cells lines. Values are normalized to *HPRT* levels using Δ cycle threshold method. $*p < 0.05$ when compared with NTC. BM, bone marrow; CB, cord blood; DC, dendritic cell; GC, germinal center; NTC, no template control; PB, peripheral blood; PBL, peripheral blood leukocyte; Treg, regulatory T cell.

and skeletal muscle. *NLRC3* has a more restricted expression profile; it is highly expressed in immunological tissues such as spleen, thymus, liver, and leukocytes. We did detect *NLRC3* in nonhematopoietic tissues such as the prostate, small intestine, and ovary, although this result might reflect tissue resident immune cells. These results are consistent with expression profiles generated by the Human Protein Atlas (62).

To further assess the possible expression profile of human *NLRC3* and *IQGAP1* in purified immune cells, we screened available microarray databases for expression profiles of *IQGAP1* and *NLRC3*. We found that the relative expression patterns of *IQGAP1* and *NLRC3* have partial overlap in the hematopoietic compartment with expression in primary lymphoid and myeloid cells (Fig. 2B, 2C). The highest relative expression of *IQGAP1* was seen in bone marrow neutrophils and peripheral blood leukocytes and the lowest relative expression was in lymphocytes; in contrast, *NLRC3* has high relative expression in lymphocytes and lower relative expression in myeloid cells.

To investigate absolute expression profiles of *NLRC3* and *IQGAPQ1* in human cells, we screened an additional database: The Gene Expression Barcode 3.0 (63). We explored the absolute expression levels of each of these transcripts in primary immune cells and tissues to determine if transcripts were silenced or expressed (63). In Fig. 2D and 2E, gene expression bar coding for immune tissues and cells is illustrated as a function of Z-scores. A Z-score above five suggests a high likelihood that a gene is expressed in that cell or tissue (63). This bar coding demonstrates that *IQGAP1* and *NLRC3* are expressed in the spleen and thymus (Fig. 2D, 2E), consistent with our expression data in Fig. 2A. However, purified cell populations are less clear. For example, *IQGAP1* has robust and significant expression in myeloid/monocytic cells (see arrows Fig. 2D). *NLRC3* has consistent expression in lymphoid cells, but the expression in myeloid cells is unclear, possibly due to its lower level of expression (see arrows in Fig. 2E). These data suggest a reciprocal and complex relationship between *IQGAP1* and *NLRC3* expression levels in single cell types, which might be dependent upon the biological roles of these proteins. QPCR analysis of *NLRC3* expression in cell lines used in this study is consistent with previous reports (51): Jurkat cells express the highest levels of *NLRC3*, whereas THP1 cells express modest amounts. HeLa cells express low but detectable levels of *NLRC3* under our experimental conditions (Fig. 2F, Table I). Despite the high relative expression of *NLRC3* in T lymphocytes there have been no published in vivo phenotypes using mouse models. Phenotypic results have only been described in myeloid and epithelial/fibroblast cells (26, 48, 52). Therefore, we have focused our initial investigation using myeloid (THP1) and epithelial cells (HeLa), which express moderate to low levels of *NLRC3*, but relatively high levels of *IQGAP1*.

IQGAP1 RGCT interacts with NLRC3 via the NBD

We investigated the potential interaction of IQGAP1 and NLRC3 in human cells by coimmunoprecipitation. We generated IQGAP1 RGCT constructs and NLRC3 truncation constructs; CARD (residues 1–60) only referred to as N, the NNBD (residues 1–646), and the NBD only (residues 61–646); to confirm the yeast two-hybrid interaction data. As shown in Fig. 3A, epitope-tagged (FLAG) IQGAP1 RGCT interacts with full-length, epitope-tagged (HA) NLRC3 but not HA-tagged IL-1β in HEK293T cells. Likewise, full-length, FLAG-tagged IQGAP1 interacts with both the NBD and NNBD of NLRC3 but not the N-terminal domain when expressed as GFP-fusion constructs. These data demonstrate that the region of NLRC3 sufficient for mediating the interaction with IQGAP1 spans amino acids 60–600, which encodes most of the NBD. This region of NLRC3 has also been shown to directly interact with STING (48). To further explore the interaction between IQGAP1 and NLRC3, we cotransfected full-length constructs into HEK293T cells. FLAG- and GFP-tagged IQGAP1 specifically interacted with HA-tagged NLRC3 but no other NLR proteins (Fig. 3C, 3D). Two related NLR proteins, NOD2 and CIITA, which contain a CARD and CARD-like regions, and NLRX1, which is involved in antiviral responses, do not interact with IQGAP1 under these conditions. Likewise, FLAG-tagged NLRC3 coimmunoprecipitates a GFP–IQGAP1 fusion construct but not GFP (Fig. 3E). These data, using multiple epitope tags and reciprocal immunoprecipitations, suggest that IQGAP1 specifically interacts with NLRC3 but no other NLR proteins (NLRX1, CIITA, or NOD2) or irrelevant proteins (GFP and IL-1β) in human epithelial cells. Although the yeast two-hybrid data suggest the NLRC3 directly interacts with IQGAP1, we cannot rule out the possibility that additional proteins may influence directly or indirectly the binding of NLRC3 to IQGAP1 in human cells.

One yeast two-hybrid screen (screen 1 in Fig. 1) and our coimmunoprecipitation (Fig. 3B) experiments in HEK293T cells suggested that the NBD of NLRC3 was sufficient to mediate an interaction with the IQGAP1 RGCT domain. The NBD of NLRs contains the highly conserved Walker A (GKS/T) and Walker B (DGLD) motifs necessary for binding and hydrolyzing nucleotide triphosphates such as ATP and GTP (64). Several NLR family members have been shown to act as ATPases or GTPases (22, 65). The nucleotide-binding cycle of NLR proteins is hypothesized to regulate NLR function by promoting homotypic oligomerization or heterologous protein interaction. To test if the nucleotide-binding cycle is involved in facilitating the binding of IQGAP1 to NLRC3, we generated mutations in the *NLRC3* cDNA. A double mutant NLRC3 consisting of Walker A (corresponding to G150 K151 → A150 A151) and Walker B mutations (D219 G220 L221 D222 → A219 G220 L221 A222) was constructed and cotransfected with FLAG-tagged IQGAP1 into HEK293T cells. This putative loss-of-function construct retains its ability to interact with IQGAP1 at similar levels as wild-type NLRC3, which suggests the predicted nucleotide-binding cycle of NLRC3 is not necessary for binding IQGAP1 (Fig. 3F).

Subcellular distribution of IQGAP1 and NLRC3

Based on the biochemical interaction between IQGAP1 and NLRC3, we were interested in exploring if NLRC3 and IQGAP1 colocalize in human cells. NLRC3 is a predicted cytosolic protein that has been shown to interact with TBK1 and STING in HEK293T cells in vitro and as purified recombinant protein in solution (48). This interaction inhibits TBK1-dependent activation of IRFs. NLRC3 has little to no effect on MAVS–dependent activation of IFN-stimulated regulatory element– and NFκ-B–dependent luciferase activity (48). IQGAP1, because of its scaffolding nature, has been implicated in many diverse processes in the cell. As such, it localizes to the cytoskeleton, the cytoplasm, and the nucleus (66). To explore the subcellular localization of these proteins, HeLa cells were transiently transfected with recombinant FLAG-tagged IQGAP1 or HA-tagged NLRC3 and visualized with confocal microscopy (Fig. 4). Consistent with previous reports, epitope-tagged IQGAP1 showed enrichment at the cell cortex but also showed diffuse cytosolic staining (Fig. 4A). Epitope-tagged NLRC3-HA showed variable subcellular distribution in individual cells. In Fig. 4B, NLRC3-HA shows diffuse cytosolic staining with regions that are consistent with the cell cortex and the endoplasmic reticulum (ER). However, over multiple transfections and different epitope tags, overexpressed NLRC3 forms discreet and large puncta or aggregates (Fig. 4C, see arrow). We were interested in determining if these puncta colocalized to the

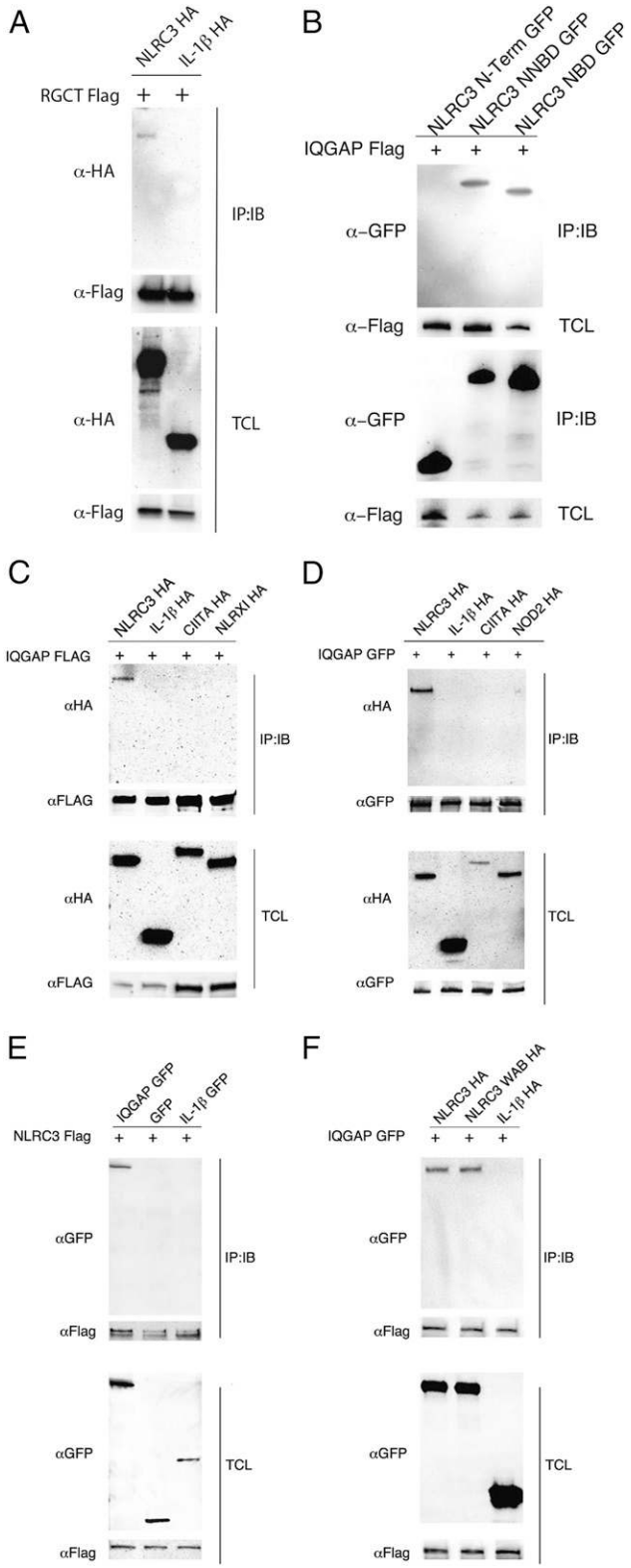

FIGURE 3. IQGAP1 specifically interacts with NLRC3 in human cells. HEK293T cells were transiently transfected with different epitope-tagged, full-length and truncated versions of IQGAP1 and NLRC3. Lysates were immunoprecipitated for IQGAP1 and immunoblots were probed to detect NLRC3 or vice versa. (**A**) The RGCT domain (amino acids 1438–1657) of IQGAP1 interacts with full-length NLRC3. (**B**) The NBD (amino acids 60–646) of NLRC3 interacts with full-length IQGAP1. (**C** and **D**) Full-length IQGAP1 (either N-terminal FLAG or GFP tagged) interacts with HA-tagged NLRC3 but not with HA-tagged IL-1β, CIITA, NLRX1, or NOD2. (**E**) Reciprocal coimmunoprecipitations confirm the interaction between IQGAP1 and NLRC3 but not an irrelevant protein such as IL-1β. (**F**) Mutations in the Walker A and Walker B motifs (WAB) do not alter the ability of NLRC3 to interact with IQGAP1. Images are representative of triplicate experiments.

ER, Golgi apparatus, or the mitochondria as these organelles have been described as signaling platforms. HeLa cells transfected with NLRC3-HA were stained with an anti–Golgin-97 Ab to detect the Golgi apparatus (Fig. 4D), cotransfected with an ER-targeted mClover fluorescent protein (Fig. 4E), or stained with an anti-Tomm20 Ab to stain the mitochondria (Fig. 4F). These puncta do not appear to colocalize with the mitochondria, there is only partial overlap with the ER, and minimal colocalization with the Golgi apparatus. These results were confirmed with SW480 cells transfected with the ColorfulCell vector (see Supplemental Fig. 2). To determine if NLRC3 and IQGAP1 colocalize in epithelial cells, we cotransfected HeLa cells. As seen in Fig. 5A, both IQGAP1 and NLRC3 show enrichment at the cell cortex (see arrow) as well as diffuse cytosolic/cytoplasmic staining. IQGAP1 has been shown to interact with both actin filaments and microtubules. We next investigated if the presumed cortical staining colocalized with actin filaments. In Fig. 5B, we counterstained with phalloidin in our cotransfected HeLa cells. In these cells, NLRC3 and IQGAP1 partially colocalize to the actin cortex, but not the microtubules (Fig. 5C). To explore this colocalization in more physiological conditions, we transfected NLRC3-HA and stained for endogenous IQGAP1. Fig. 5D shows distinct and robust colocalization of NLRC3-HA with endogenous IQGAP1 (see inset). We have not been able to find a suitable NLRC3 Ab that works well in immunofluorescence, so we have been unable to detect endogenous NLRC3. HeLa cells that have been transduced with an shRNA scramble sequence (Fig. 5E) and an shRNA that targets *IQGAP1* (Fig. 5F) were used to show that our staining of endogenous IQGAP1 is specific (see also Supplemental Fig. 1). When these HeLa cells are transfected with NLRC3-HA we see a reduced amount of localization to the cell cortex (see arrow in Fig. 5E) in the absence (or reduction) of endogenous *IQGAP1*. These data suggest that NLRC3 can be localized to the cell cortex, possibly via interactions with IQGAP1. These data are consistent with previous studies on IQGAP1, but a novel finding for NLRC3.

To confirm our confocal microscopy data, we performed biochemical subcellular fractionation by differential lysis on SW480 cells transfected with IQGAP1, NLRC3, or both constructs to determine if localization is altered by either protein. In Fig. 6G, we show that NLRC3 and IQGAP1 have diverse subcellular distributions in single transfections. These proteins localize to the cytosol, membrane, nucleus, and cytoskeleton. In a small percentage of cells we have observed NLRC3 localized to the nucleus (data not shown). There are several reported instances of unexpected nuclear localization of presumably cytosolic NLRs such as NOD2 and NLRP3 (33, 67); this result might reflect a generalized ability of NLR proteins to translocate into the nucleus. Consistent with our microscopy data, there is a fraction of the pool of NLRC3 proteins that is distributed to the cytoskeleton fraction. The relative amount of cytoskeletal NLRC3 varied between independent experiments, but was always present. We detect a small relative amount of IQGAP1 in the cytoskeletal fraction, as predicted. However, the amount of cytoskeletal IQGAP1 increases in the presence of cotransfected NLRC3.

NLRC3 has been shown to interact with TBK1 and STING and possibly disrupts the redistribution of STING from the MAM to the perinuclear region (18, 68). We next investigated if known

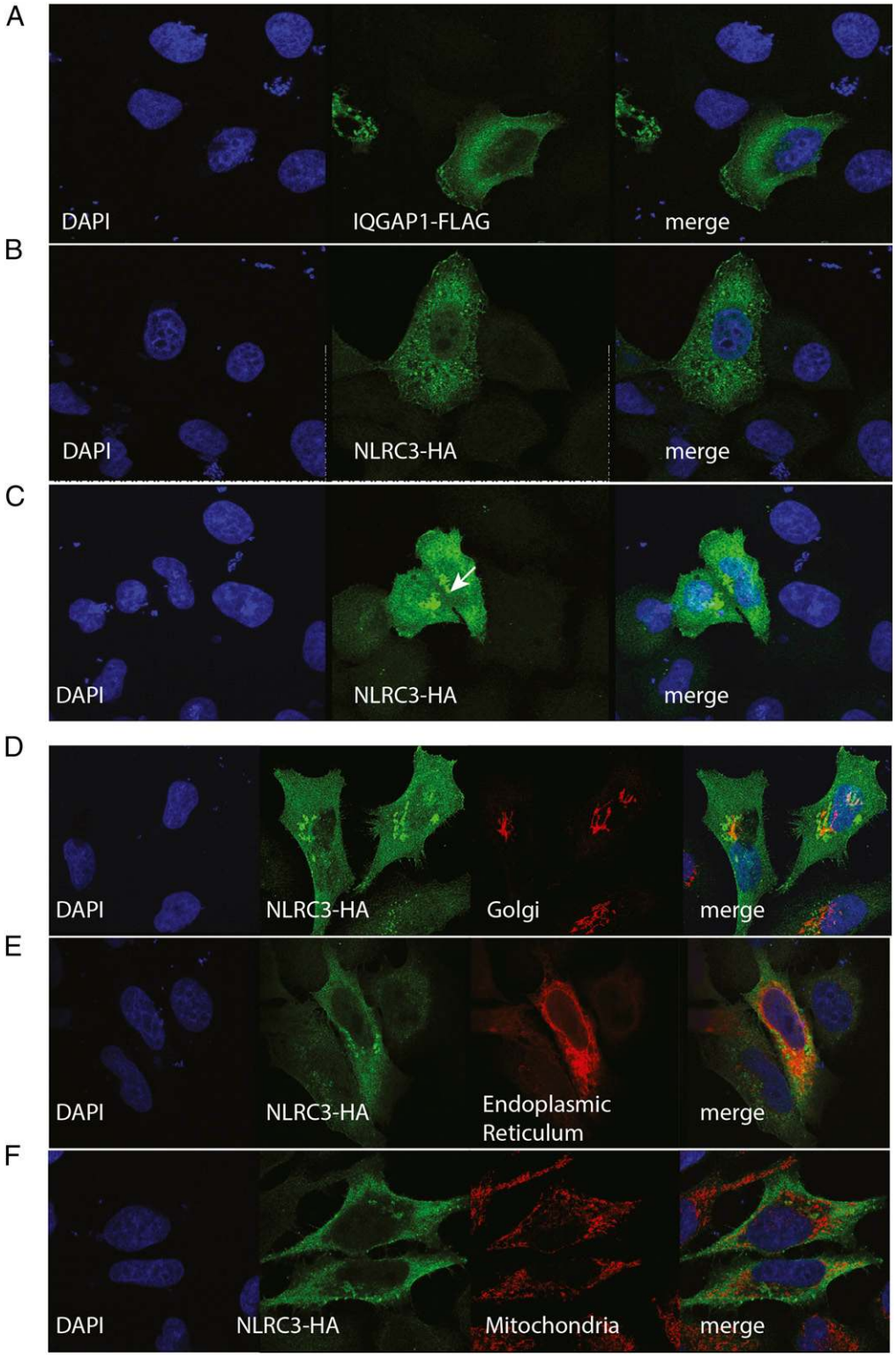

FIGURE 4. Confocal microscopy of HeLa cells transfected with epitope-tagged IQGAP1-FLAG (**A**) or NLRC3-HA (**B** and **C**). Cells were fixed, permeabilized, and stained with Abs specific to the epitope tag followed by species-specific Alexa Fluor 488 and Alexa 568 secondary Abs and DAPI to counterstain the nucleus. Cells are representative of more than three independent transfections. The Golgi apparatus (**D**) was stained with anti–Golgin-97 Ab; an ER-specific fluorescent protein (Plasmid 56310; Addgene) was used to highlight the ER (**E**), whereas mitochondria were identified with an anti-Tomm20 Ab (**F**). Images were collected using a 63× 1.4 numerical aperture oil immersion objective lens.

NLRC3-interacting proteins colocalized to specific regions in HeLa cells. FLAG-tagged TBK1, V5-tagged STING, and FLAG-tagged MAVS were transfected with NLRC3-HA (see Fig. 6) and counterstained with Abs to endogenous IQGAP1. Transfected STING constructs show two distinct staining patterns that may reflect its activation status. Fig. 6A shows putatively active STING and panel B shows STING with ER staining typical of nonactivated STING. The localization of all of these proteins occurred in the absence of stimulation; however, overexpressed proteins might be aberrantly activated signaling pathways. These data possibly do

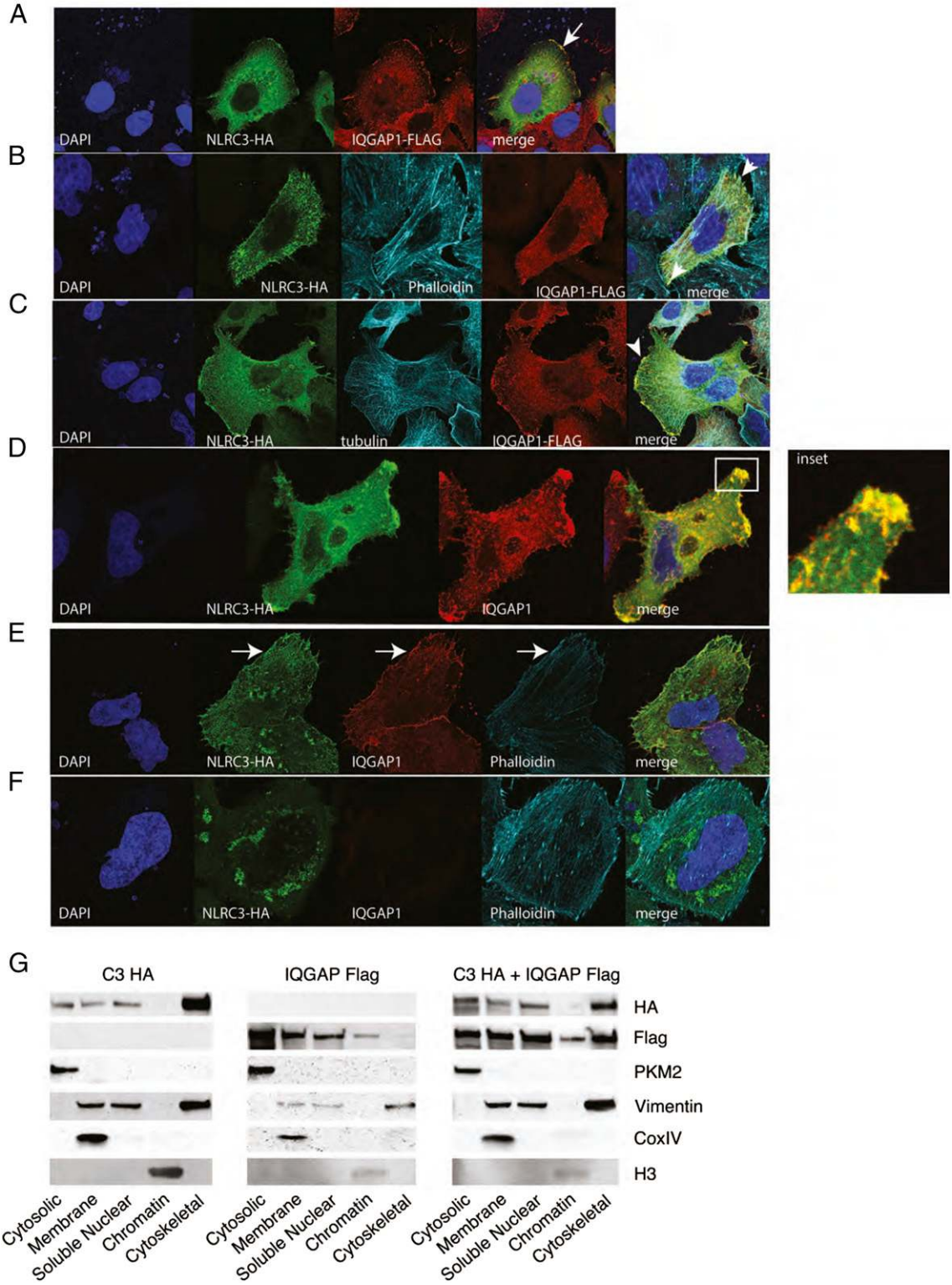

FIGURE 5. Confocal microscopy of HeLa cells cotransfected with FLAG-tagged IQGAP1 and HA-tagged NLRC3 (**A**) and stained for endogenous proteins: (**B**) phalloidin conjugated to Alexa 647, (**C**) tubulin, (**D**) endogenous IQGAP1. Cells were counterstained with DAPI to visualize the nucleus. Boxed inset in (D) shows robust cortical colocalization with NLRC3. (**E**) shRNA scramble. (**F**) shIQGAP1 HeLa cells were transfected with NLRC3-HA and stained for endogenous IQGAP1 and epitope-tagged NLRC3 and phalloidin. Arrows represent cortical actin staining of NLRC3 and IQGAP1 in (E). Images were collected using a 63× 1.4 numerical aperture oil immersion objective lens. (**G**) SW480 cells were transfected with epitope-tagged NLRC3, epitope-tagged IQGAP1, and cotransfected. Cells were fractionated using subcellular fractionation kit. Immunoblots were probed with Abs to specific proteins in each fraction. Images are representative of at least three individual replicates.

not differentiate between homeostatic versus activation-induced interaction or localizations. NLRC3 and IQGAP1 showed minimal to no colocalization with MAVS in HeLa cells (Fig. 6D). Either form of STING (Fig. 6A, 6B) did not colocalize to the cell cortex along with a fraction of NLRC3 and IQGAP1. TBK1 showed diffuse cytosolic or cytoplasmic staining that did not clearly colocalize at the cortex with IQGAP1 and NLRC3 (Fig. 6A–C). However, there is a portion of the cellular pool of

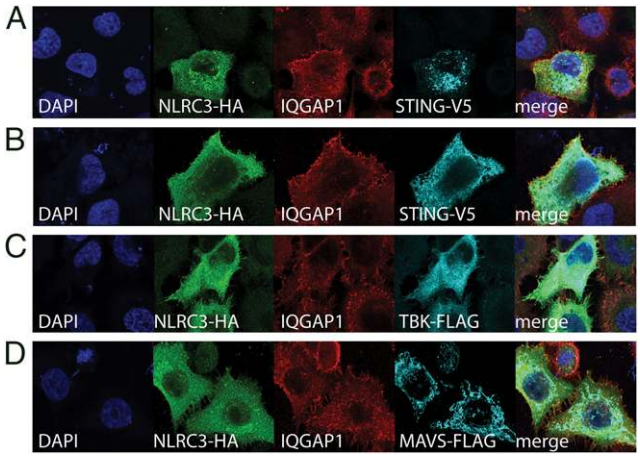

FIGURE 6. IQGAP1 and NLRC3 show partial colocalization with recombinant STING, TBK1, and not MAVS. HeLa cells were transiently transfected with different expression constructs. (**A**–**D**) Confocal microscopy of HeLa cells cotransfected with NLRC3 and associated expression constructs. Cells were fixed, permeabilized, and stained with Abs specific to the epitope tags and endogenous IQGAP1 followed by species-specific Alexa Fluor 488, Alexa Fluor 568, and Alexa 647 secondary Abs and DAPI to counterstain the nucleus. Cells are representative of more than three independent transfections. Images were collected using a 63× 1.4 numerical aperture oil immersion objective lens. (A and B) show two distinct colocalization patterns of STING: (A) puncta and (B) ER.

both IQGAP1 and NLRC3 that has diffuse cytosolic/cytoplasmic staining which might colocalize with TBK1 and/or STING. These data suggest that there might be individual pools of NLRC3 that interact with different signaling or scaffolding proteins.

IQGAP1 is involved in cytosolic nucleotide sensing and type I IFN production

We chose to use THP1 and HeLa cells to investigate the functional significance of the NLRC3 and IQGAP1 interaction in vitro. THP1 cells have been shown to express both *NLRC3* and *IQGAP1* (see Fig. 2F, Supplemental Fig. 1). Additionally, the function of NLRC3 has been investigated using THP1 cells as well as mouse bone marrow–derived macrophages (52) and mouse embryonic fibroblasts (48). We generated IQGAP1 shRNA knockdown in THP1, THP1-Dual, and HeLa cells (Fig. 7). THP1-Dual Cells are engineered with a secreted luciferase (*Lucia*) gene fused to the *ISG54* minimal promoter with five tandem IFN-stimulated regulatory elements and a *SEAP* gene driven by the minimal IFN-β promoter fused to five NF-κB responsive sites and three c-Rel binding sites to allow for rapid detection of both IRF- and NF-κB–dependent transcription. We investigated the role of IQGAP1 in all three cell lines. First, we investigated if IQGAP1 is necessary for regulated responses to intracellular nucleic acids that are potent activators of type I IFN. To this end, we stimulated THP1, THP1-Dual, and HeLa shRNA cells with transfected dicyclic nucleotides (2′2 ′ and 3′3′ cGAMP) or immunostimulatory DNA, and measured IFN-β secretion (Fig. 7A, 7C) or Lucia activity (Fig. 7B). In the absence (or with significant reduction) of IQGAP1, all cell lines secreted significantly higher levels of IFN-β (or ISG54-driven Lucia). NLRC3 has also been shown to affect proinflammatory cytokine secretion during a cecal ligation puncture model of experimental colitis (52). We next stimulated THP1 (Fig. 7D) and THP1-Dual (Fig. 7E) cells with bacterial PAMPs to induce a NF-κB–dependent proinflammatory cytokine response and measured IL-6 or IL-1β production. IQGAP1 appears to be dispensable for TLR responses, as there was no significant difference between *IQGAP1* knockdown and scramble

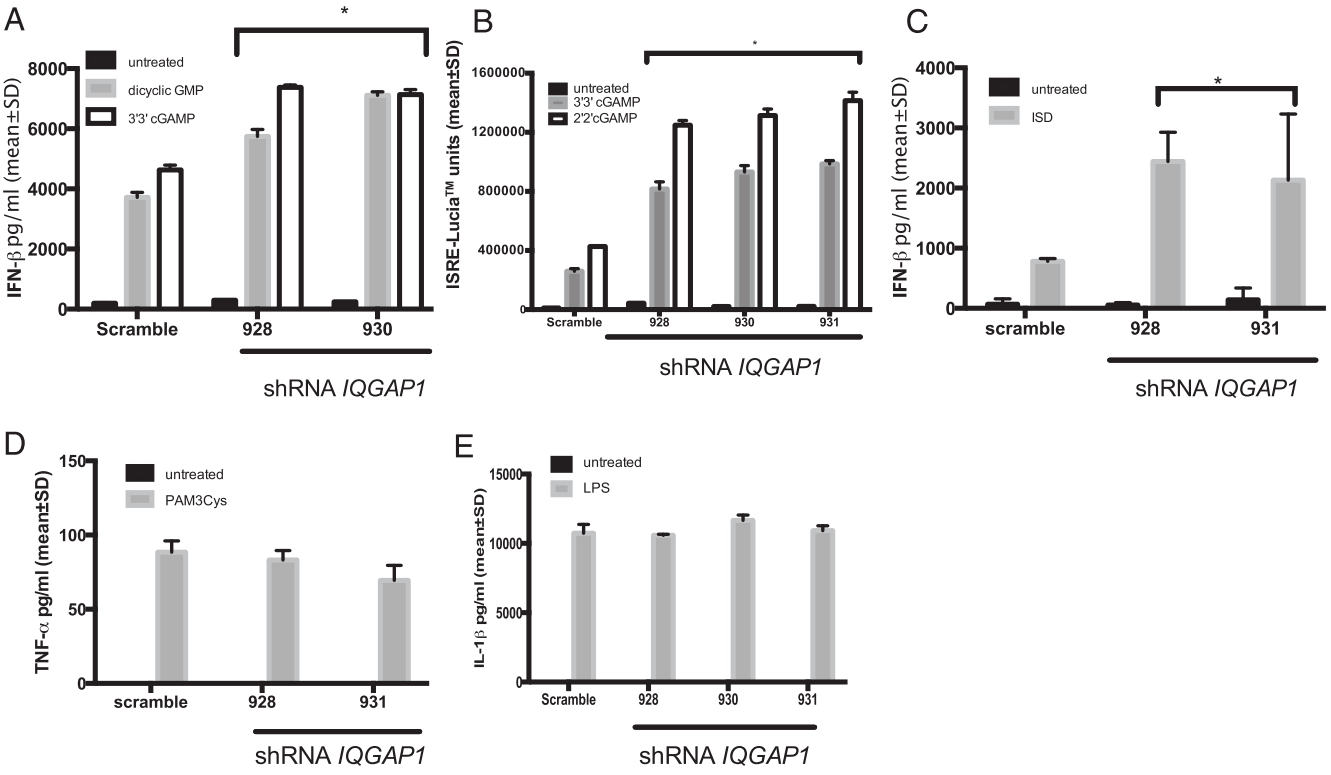

FIGURE 7. shRNA-mediated knockdown of *IQGAP1* in different cell lines induces hyperactivation of the IFN-β pathway. (**A**–**C**) Stable integrants [(A) and (**D**) represent THP-1 cells, (B) and (**E**) represent THP1-Dual Cells, and (C) represents HeLa cells] were selected and stimulated as indicated. IFN or cytokine levels were measured by ELISA and secreted Lucia. Values represent mean ± SD of triplicate samples. Data are representative of at least three biological replicates. (D) and (E) show no significant differences relative to the scramble shRNA. *$p < 0.05$ when compared with scramble shRNA cells.

cells. These data suggest that IQGAP1 functions specifically to inhibit the production of type 1 IFN and not proinflammatory cytokines.

IQGAP1 disrupts the NLRC3–STING interaction

Our colocalization studies (see Fig. 5A–F) clearly demonstrate at least a portion of the cellular pool of NLRC3 is localized to the cell cortex, but this localization appears to be independent of STING and TBK1 (Fig. 6A–C). This observation coupled with the overlapping interaction location of both STING and IQGAP1 to the NBD of NLRC3 led us to speculate that IQGAP1 could regulate the NLRC3–STING complex. To explore this possible mechanism, we examined if increasing amounts of overexpressed IQGAP1 could modulate the interaction of NLRC3 with STING. As shown in Fig. 8A, in the presence of overexpressed IQGAP1, NLRC3 no longer interacts with overexpressed STING. We next investigated if IQGAP1 could interact with STING in the absence of overexpressed NLRC3. Under two different stringencies, we were unable to detect STING interaction with IQGAP1 (see Fig. 8B). These data suggest that IQGAP1 has the ability to interact with NLRC3, and this interaction can affect the NLRC3–STING interaction. How these dynamic interactions negatively regulate type 1 IFN production is not well understood.

Discussion

Macrophages and epithelial cells detect cytosolic nucleotides and mount a robust type I IFN (IFN-α/β) response to limit pathogen spread. Cells respond by activating the IRF family of transcription factors to induce the antiviral transcriptome. TBK1 is the keystone kinase that integrates numerous upstream cytosolic nucleic acid sensors. TBK1 phosphorylates IRF3 and/or IRF7, which allows it to dimerize and translocate into the nucleus. One upstream sensor in particular, cGAS, directly binds cytosolic DNA to generate dicyclic nucleotides. These intermediates can directly bind to STING, allowing it to activate TBK1. However, sustained or aberrant type I IFN production is associated with several autoimmune and autoinflammatory diseases: broadly termed IFNopathies (69). Distinct host pathways, such as miR-146a (70), SOCS-1 (71), and DUBA (72), among others (73), can downregulate type I IFN responses, possibly to limit immunopathology associated with overzealous responses. STING is targeted for degradation via multiple pathways. UNC-51–like kinase (ULK1) has been shown to phosphorylate STING at S366 to facilitate its lysosomal degradation in a negative-feedback loop to inhibit prolonged responses (17). Additionally, RNF5 facilitates K48-linked ubiquitination of STING on the K150 residue after viral infection. This modification allows for ubiquitin-dependent proteosomal degradation (19). Previously, NLRC3 has been shown to inhibit type I IFN production by disrupting the dynamic redistribution of STING between the ER and MAM and inhibiting its interaction with TBK1 (48). However, the molecular mechanisms that control NLRC3 inhibition of STING remain poorly characterized. In this study, we have shown that NLRC3 interacts with IQGAP1 using a yeast two-hybrid screen and coimmunoprecipitation experiments in human cell lines. We identified a C-terminal fragment of IQGAP1 that specifically interacts with the NBD, albeit independently of the nucleotide-binding cycle, of NLRC3 (Fig. 3). The RGCT domain of IQGAP1 has been shown to interact with multiple protein partners, for example, E-cadherin, β-catenin, Clip170, cytoplasmic linker–associated protein 2 (Clasp2), and adenomatous polyposis coli (74). The RGCT domain is responsible for anchoring IQGAP1 to the membrane at the cell periphery and has been shown to dynamically bind small GTPases, such as Cdc42, in a phosphorylation-dependent manner at the leading edge of the plasma membrane (75).

IQGAP1 regulates many diverse cellular processes in different cell types and tissues, notably in cell motility and invasion via cytoskeletal rearrangement, but also cotranscriptional regulation with β-catenin. NLRC3 and IQGAP1 have similar, but not necessarily overlapping, expression profiles in unstimulated cells. Both have increased relative expression in lymphocyte and myeloid cells, further suggesting a possible endogenous role in vivo (Fig. 2). Additionally, both NLRC3 and IQGAP1 are expressed, albeit at low levels for NLRC3, in epithelial cells. We have demonstrated that NLRC3 and IQGAP1 colocalize in human epithelial cells (Figs. 4–6). In the adaptive immune system, IQGAP1 negatively regulates TCR signaling and F-actin dynamics. In the absence of IQGAP1, Jurkat T cells and primary mouse T lymphocytes secrete significantly more IL-2 and IFN-γ (54). It is interesting to note that knockdown of NLRC3 in Jurkat T cells also shows increased IL-2 production and CD25 expression levels (51). This effect might be mediated via IQGAP1, but this hypothesis remains to be tested. In macrophages, mouse IQGAP1 has been shown to be important in phagocytosis and phagocytic cup formation in macrophages during incubation with avidin-coated beads (76) and LPS-induced Rac1 activation during phagocytosis (77). This effect requires the interaction of IQGAP1 with the actin nucleating protein, diaphanous-related formin (Dia1). The rearrangement of the host cell cytoskeleton is a crucial mechanism by which invasive bacteria enter cells. The pathogenic bacterium, *Salmonella enterica*, co-opts IQGAP1 to alter Rac1 and MAPK signaling to facilitate chronic infection in epithelial cells (78), suggesting that IQGAP1 is necessary for invasion.

The movement of signaling proteins in sensing cytosolic nucleic acids is dynamic and highly coordinated. The activated STING/TBK1 complex is trafficked from the ER and Golgi apparatus, via ATG9, to the endosomes/lysosomes containing IRF and NF-κB

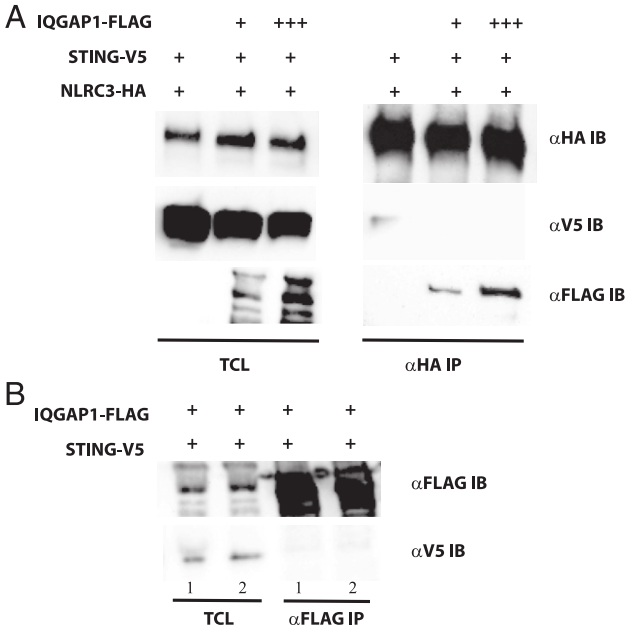

FIGURE 8. IQGAP1 sequesters NLRC3 to the actin cytoskeleton. (**A**) HEK293T cells were transiently transfected with epitope-tagged IQGAP1, NLRC3, and STING. Lysates were immunoprecipitated for NLRC3-HA and blotted for interacting proteins. Data are representative of three replicates. (**B**) IQGAP1 and STING were cotransfected in the absence of NLRC3-HA, immunoprecipitated for IQGAP1, and blotted for STING. Cells were lysed in stringent (PBS with 1% Triton X-100 with 0.5% sodium deoxycholate shown in lane 1) and less stringent (PBS with 1% Triton X-100 shown in lane 2) conditions. Data are representative of three replicates.

Table I. Sequences of primers used

Gene	Forward Primer (5′→3′)	Reverse Primer (5′→3′)
IQGAP1 full length	ATGTCCGCCGCAGACGAGGTTGACGGGC	TTACTTCCCGTAGAACTTTTTGTTGAGAAGG
IQGAP1 RGCT	ATGAAAAAGTCAAAATCTGTAAAGG	TTACTTCCCGTAGAACTTTTTGTTGAGAAGG
NLRC3 full length	ATGAGGAAGCAAGAGGTGCGGACGGGC	TCACATTTCAACAGTGCACGTGGGAGC
NLRC3 N-terminal	ATGAGGAAGCAAGAGGTGCGGACGGGC	GTCATTGCTGCAGGGCCCCAGC
NLRC3 NBD	TCAAGGATACAGAGGCACCGCAAGGCCC	GTCCAGCCTGAGCTTCCGGCAGTAGAGC
NLRC3 NNBD	ATGAGGAAGCAAGAGGTGCGGACGGGC	GTCCAGCCTGAGCTTCCGGCAGTAGAGC
QPCR NLRC3	CGGAGAACCAGATCAGTAACAA	CCTTGTGGTCCAATGGAGTTA
QPCR HPRT	TGACACTGGCAAAACAATGCA	GGTCCTTTTCACCAGCAAGCT

transcription factors in a VPS34-dependent manner (17). Movement of STING is thought to be mediated via posttranslational palmitoylation at two key cysteine residues (C88 and C91) at the Golgi apparatus (79). This trafficking allows for efficient transcription factor activation and the subsequent antiviral transcriptional program. TBK1 molecules are recruited to larger macromolecular signaling complexes upon activation via interactions with scaffolding and adaptor proteins such as TANK, SINTBAD, NAP1, TAPE, and IFIT3 (80). The latter two of which are involved in TBK1-dependent type I IFN production in response to viral infection. Specifically, TBK1 has been shown to relocate from the cytosol to mitochondria in response to DNA virus infection or transfection of DNA into the cytosol of HeLa and HepG2 cells, but not RAW264.7, L929, or T-23 cells (81). These data suggest that TBK1 subcellular localization is cell-type or stimulus dependent. This clustering of TBK1 to specific subcellular locations facilitates autophosphorylation and subsequent substrate targeting. Nonetheless, the mechanisms by which TBK1 and STING dynamically redistribute within the subcellular space are largely unknown. Our data suggest that IQGAP1 with its known scaffolding ability, its diverse subcellular distribution, and its novel interaction with NLRC3 might function to regulate TBK1 or STING activity or location and downstream activation of the IRF3 and/or IRF7.

The subcellular localization of NLR proteins is as diverse as the cellular pathways with which they are associated. NOD2 has been shown to localize to the plasma membrane via interactions with ERBIN (67, 82) and FRMBP2 (83). Additionally, NOD2 has been shown to localize to endosomes (possibly via SLC15A3 or SLC15A4) in dendritic cells (84) and autophagosomes (via ATG16L1) in HeLa cells and MEFs (85) in response to invasive bacterial infection or stimulation with the bacterial PAMP muramyl dipeptide, the known ligand for NOD2. Also, NOD2 has been shown to localize to the mitochondria where it interacts with MAVS in response to ssRNA virus (36). The molecular mechanisms by which NOD2 is distributed to different subcellular locations is not well understood, and how the subcellular distribution relates to the pathophysiology related to the NOD2-dependend pathologies (Crohn's disease and early onset sarcoidosis) is under investigation. Surprisingly, we show that a portion of NLRC3 is localized to the cell cortex in HeLa cells, possibly via its interaction with IQGAP1, a known actin- and tubulin-binding protein. How this specific subcellular localization affects NLRC3 function is unknown but might relate to compartmentalization or sequestration of signaling molecules to inhibit or dampen chronic or aberrant activation of the type I IFN pathway.

We show that IQGAP1 is necessary for appropriate responses to cytosolic nucleotides. Type I IFN production was significantly increased in THP1 and HeLa cells that stably express shRNA to IQGAP1. However, this effect was specific for type I IFN; THP1 cells expressing shRNA to IQGAP1 did not secrete significantly different amounts of proinflammatory cytokines, IL-1β, or TNF-α. A limitation of our studies is the reliance on ectopic and overexpression of IQGAP1, NLRC3 and TBK1 in particular, and small interfering RNA. In an attempt to overcome these limitations we used human HAP1 cells that were engineered via Cas9/CRISPR to be deficient in IQGAP1. In our experiments, the parental HAP1 cell line was refractory to stimulation with immunostimulatory nucleic acids and was not amenable to transfection (data not shown). Nonetheless, to our knowledge, our data are the first to demonstrate that IQGAP1 negatively regulates type I IFN production, possibly via its interaction with NLRC3. The role of IQGAP1 as a scaffolding protein is well documented, and the ability of NLRC3 to interact with the RGCT domain adds to the growing number of IQGAP1-interacting proteins. These data help better define the molecular mechanisms of NLR-mediated IFN inhibition that is necessary to maintain homeostasis. Investigating the role of additional regulatory proteins in the NLR–IFN axis will be critical to our understanding of host–pathogen interactions.

Acknowledgments

We thank Jenny P.Y. Ting, University of North Carolina, for the plasmids encoding MAVS, STING, and TBK1. We are grateful to Wade Edris for technical assistance with confocal microscopy at the Imaging Core at Penn State College of Medicine and Heather Hoffmann for technical assistance.

Disclosures

The authors have no financial conflicts of interest.

References

1. Cui, J., Y. Chen, H. Y. Wang, and R. F. Wang. 2014. Mechanisms and pathways of innate immune activation and regulation in health and cancer. *Hum. Vaccin. Immunother.* 10: 3270–3285.
2. Barton, G. M., and J. C. Kagan. 2009. A cell biological view of Toll-like receptor function: regulation through compartmentalization. *Nat. Rev. Immunol.* 9: 535–542.
3. Schneider, W. M., M. D. Chevillotte, and C. M. Rice. 2014. Interferon-stimulated genes: a complex web of host defenses. *Annu. Rev. Immunol.* 32: 513–545.
4. Ablasser, A., M. Goldeck, T. Cavlar, T. Deimling, G. Witte, I. Röhl, K. P. Hopfner, J. Ludwig, and V. Hornung. 2013. cGAS produces a 2′-5′-linked cyclic dinucleotide second messenger that activates STING. *Nature* 498: 380–384.
5. Civril, F., T. Deimling, C. C. de Oliveira Mann, A. Ablasser, M. Moldt, G. Witte, V. Hornung, and K. P. Hopfner. 2013. Structural mechanism of cytosolic DNA sensing by cGAS. *Nature* 498: 332–337.
6. Diner, E. J., D. L. Burdette, S. C. Wilson, K. M. Monroe, C. A. Kellenberger, M. Hyodo, Y. Hayakawa, M. C. Hammond, and R. E. Vance. 2013. The innate immune DNA sensor cGAS produces a noncanonical cyclic dinucleotide that activates human STING. *Cell Reports* 3: 1355–1361.
7. Huang, Y. H., X. Y. Liu, X. X. Du, Z. F. Jiang, and X. D. Su. 2012. The structural basis for the sensing and binding of cyclic di-GMP by STING. *Nat. Struct. Mol. Biol.* 19: 728–730.
8. Ouyang, S., X. Song, Y. Wang, H. Ru, N. Shaw, Y. Jiang, F. Niu, Y. Zhu, W. Qiu, K. Parvatiyar, et al. 2012. Structural analysis of the STING adaptor protein reveals a hydrophobic dimer interface and mode of cyclic di-GMP binding. *Immunity* 36: 1073–1086.
9. Yin, Q., Y. Tian, V. Kabaleeswaran, X. Jiang, D. Tu, M. J. Eck, Z. J. Chen, and H. Wu. 2012. Cyclic di-GMP sensing via the innate immune signaling protein STING. *Mol. Cell* 46: 735–745.
10. Shang, G., D. Zhu, N. Li, J. Zhang, C. Zhu, D. Lu, C. Liu, Q. Yu, Y. Zhao, S. Xu, and L. Gu. 2012. Crystal structures of STING protein reveal basis for recognition of cyclic di-GMP. *Nat. Struct. Mol. Biol.* 19: 725–727.

11. Shu, C., G. Yi, T. Watts, C. C. Kao, and P. Li. 2012. Structure of STING bound to cyclic di-GMP reveals the mechanism of cyclic dinucleotide recognition by the immune system. *Nat. Struct. Mol. Biol.* 19: 722–724.
12. Konno, H., and G. N. Barber. 2014. The STING controlled cytosolic-DNA activated innate immune pathway and microbial disease. *Microbes Infect.* 16: 998–1001.
13. Hansen, K., T. Prabakaran, A. Laustsen, S. E. Jørgensen, S. H. Rahbæk, S. B. Jensen, R. Nielsen, J. H. Leber, T. Decker, K. A. Horan, et al. 2014. Listeria monocytogenes induces IFNβ expression through an IFI16-, cGAS- and STING-dependent pathway. *EMBO J.* 33: 1654–1666.
14. Wassermann, R., M. F. Gulen, C. Sala, S. G. Perin, Y. Lou, J. Rybniker, J. L. Schmid-Burgk, T. Schmidt, V. Hornung, S. T. Cole, and A. Ablasser. 2015. *Mycobacterium tuberculosis* differentially activates cGAS- and inflammasome-dependent intracellular immune responses through ESX-1. *Cell Host Microbe* 17: 799–810.
15. Watson, R. O., S. L. Bell, D. A. MacDuff, J. M. Kimmey, E. J. Diner, J. Olivas, R. E. Vance, C. L. Stallings, H. W. Virgin, and J. S. Cox. 2015. The cytosolic sensor cGAS detects *Mycobacterium tuberculosis* DNA to induce type I interferons and activate autophagy. *Cell Host Microbe* 17: 811–819.
16. Collins, A. C., H. Cai, T. Li, L. H. Franco, X. D. Li, V. R. Nair, C. R. Scharn, C. E. Stamm, B. Levine, Z. J. Chen, and M. U. Shiloh. 2015. Cyclic GMP-AMP synthase is an innate immune DNA sensor for *Mycobacterium tuberculosis. Cell Host Microbe* 17: 820–828.
17. Konno, H., K. Konno, and G. N. Barber. 2013. Cyclic dinucleotides trigger ULK1 (ATG1) phosphorylation of STING to prevent sustained innate immune signaling. *Cell* 155: 688–698.
18. Ishikawa, H., Z. Ma, and G. N. Barber. 2009. STING regulates intracellular DNA-mediated, type I interferon-dependent innate immunity. *Nature* 461: 788–792.
19. Zhong, B., L. Zhang, C. Lei, Y. Li, A. P. Mao, Y. Yang, Y. Y. Wang, X. L. Zhang, and H. B. Shu. 2009. The ubiquitin ligase RNF5 regulates antiviral responses by mediating degradation of the adaptor protein MITA. *Immunity* 30: 397–407.
20. Ma, Z., S. R. Jacobs, J. A. West, C. Stopford, Z. Zhang, Z. Davis, G. N. Barber, B. A. Glaunsinger, D. P. Dittmer, and B. Damania. 2015. Modulation of the cGAS-STING DNA sensing pathway by gammaherpesviruses. *Proc. Natl. Acad. Sci. USA* 112: E4306–E4315.
21. Schlee, M., and G. Hartmann. 2016. Discriminating self from non-self in nucleic acid sensing. *Nat. Rev. Immunol.* 16: 566–580.
22. Mo, J., J. P. Boyle, C. B. Howard, T. P. Monie, B. K. Davis, and J. A. Duncan. 2012. Pathogen sensing by nucleotide-binding oligomerization domain-containing protein 2 (NOD2) is mediated by direct binding to muramyl dipeptide and ATP. *J. Biol. Chem.* 287: 23057–23067.
23. Hong, M., S. I. Yoon, and I. A. Wilson. 2012. Structure and functional characterization of the RNA-binding element of the NLRX1 innate immune modulator. *Immunity* 36: 337–347.
24. Halff, E. F., C. A. Diebolder, M. Versteeg, A. Schouten, T. H. Brondijk, and E. G. Huizinga. 2012. Formation and structure of a NAIP5-NLRC4 inflammasome induced by direct interactions with conserved N- and C-terminal regions of flagellin. *J. Biol. Chem.* 287: 38460–38472.
25. Davis, B. K., H. Wen, and J. P. Ting. 2011. The inflammasome NLRs in immunity, inflammation, and associated diseases. *Annu. Rev. Immunol.* 29: 707–735.
26. Karki, R., S. M. Man, R. K. S. Malireddi, S. Kesavardhana, Q. Zhu, A. R. Burton, B. R. Sharma, X. Qi, S. Pelletier, P. Vogel, et al. 2016. NLRC3 is an inhibitory sensor of PI3K-mTOR pathways in cancer. *Nature.* 540: 583–587.
27. Koblansky, A. A., A. D. Truax, R. Liu, S. A. Montgomery, S. Ding, J. E. Wilson, W. J. Brickey, M. Mühlbauer, R. M. McFadden, P. Hu, et al. 2016. The innate immune receptor NLRX1 functions as a tumor suppressor by reducing colon tumorigenesis and key tumor-promoting signals. *Cell Reports* 14: 2562–2575.
28. Li, H., S. Zhang, F. Li, and L. Qin. 2016. NLRX1 attenuates apoptosis and inflammatory responses in myocardial ischemia by inhibiting MAVS-dependent NLRP3 inflammasome activation. *Mol. Immunol.* 76: 90–97.
29. Coutermarsh-Ott, S., A. Simmons, V. Capria, T. LeRoith, J. E. Wilson, B. Heid, C. W. Philipson, Q. Qin, R. Hontecillas-Magarzo, J. Bassaganya-Riera, et al. 2016. NLRX1 suppresses tumorigenesis and attenuates histiocytic sarcoma through the negative regulation of NF-κB signaling. *Oncotarget* 7: 33096–33110.
30. Eitas, T. K., W. C. Chou, H. Wen, D. Gris, G. R. Robbins, J. Brickey, Y. Oyama, and J. P. Ting. 2014. The nucleotide-binding leucine-rich repeat (NLR) family member NLRX1 mediates protection against experimental autoimmune encephalomyelitis and represses macrophage/microglia-induced inflammation. *J. Biol. Chem.* 289: 4173–4179.
31. Wang, Y. G., W. L. Fang, J. Wei, T. Wang, N. Wang, J. L. Ma, and M. Shi. 2013. The involvement of NLRX1 and NLRP3 in the development of nonalcoholic steatohepatitis in mice. *J. Chin. Med. Assoc.* 76: 686–692.
32. Lei, Y., H. Wen, Y. Yu, D. J. Taxman, L. Zhang, D. G. Widman, K. V. Swanson, K. W. Wen, B. Damania, C. B. Moore, et al. 2012. The mitochondrial proteins NLRX1 and TUFM form a complex that regulates type I interferon and autophagy. *Immunity* 36: 933–946.
33. Bruchard, M., C. Rebé, V. Derangère, D. Togbé, B. Ryffel, R. Boidot, E. Humblin, A. Hamman, F. Chalmin, H. Berger, et al. 2015. The receptor NLRP3 is a transcriptional regulator of TH2 differentiation. *Nat. Immunol.* 16: 859–870.
34. Coutermarsh-Ott, S., K. Eden, and I. C. Allen. 2016. Beyond the inflammasome: regulatory NOD-like receptor modulation of the host immune response following virus exposure. *J. Gen. Virol.* 97: 825–838.
35. Allen, I. C. 2014. Non-inflammasome forming NLRs in inflammation and tumorigenesis. *Front. Immunol.* 5: 169.
36. Sabbah, A., T. H. Chang, R. Harnack, V. Frohlich, K. Tominaga, P. H. Dube, Y. Xiang, and S. Bose. 2009. Activation of innate immune antiviral responses by Nod2. *Nat. Immunol.* 10: 1073–1080.
37. Zou, P. F., M. X. Chang, Y. Li, N. N. Xue, J. H. Li, S. N. Chen, and P. Nie. 2016. NOD2 in zebrafish functions in antibacterial and also antiviral responses via NF-κB, and also MDA5, RIG-I and MAVS. *Fish Shellfish Immunol.* 55: 173–185.
38. Kim, Y. G., J. H. Park, T. Reimer, D. P. Baker, T. Kawai, H. Kumar, S. Akira, C. Wobus, and G. Núñez. 2011. Viral infection augments Nod1/2 signaling to potentiate lethality associated with secondary bacterial infections. *Cell Host Microbe* 9: 496–507.
39. Jing, H., L. Fang, D. Wang, Z. Ding, R. Luo, H. Chen, and S. Xiao. 2014. Porcine reproductive and respiratory syndrome virus infection activates NOD2-RIP2 signal pathway in MARC-145 cells. *Virology* 458–459: 162–171.
40. Kapoor, A., M. Forman, and R. Arav-Boger. 2014. Activation of nucleotide oligomerization domain 2 (NOD2) by human cytomegalovirus initiates innate immune responses and restricts virus replication. *PLoS One* 9: e92704.
41. Vissers, M., T. Remijn, M. Oosting, D. J. de Jong, D. A. Diavatopoulos, P. W. Hermans, and G. Ferwerda. 2012. Respiratory syncytial virus infection augments NOD2 signaling in an IFN-β-dependent manner in human primary cells. *Eur. J. Immunol.* 42: 2727–2735.
42. Allen, I. C., C. B. Moore, M. Schneider, Y. Lei, B. K. Davis, M. A. Scull, D. Gris, K. E. Roney, A. G. Zimmermann, J. B. Bowzard, et al. 2011. NLRX1 protein attenuates inflammatory responses to infection by interfering with the RIG-I-MAVS and TRAF6-NF-κB signaling pathways. *Immunity* 34: 854–865.
43. Moore, C. B., D. T. Bergstralh, J. A. Duncan, Y. Lei, T. E. Morrison, A. G. Zimmermann, M. A. Accavitti-Loper, V. J. Madden, L. Sun, Z. Ye, et al. 2008. NLRX1 is a regulator of mitochondrial antiviral immunity. *Nature* 451: 573–577.
44. Guo, H., R. König, M. Deng, M. Riess, J. Mo, L. Zhang, A. Petrucelli, S. M. Yoh, B. Barefoot, M. Samo, et al. 2016. NLRX1 sequesters STING to negatively regulate the interferon response, thereby facilitating the replication of HIV-1 and DNA viruses. *Cell Host Microbe* 19: 515–528.
45. Barouch, D. H., K. Ghneim, W. J. Bosche, Y. Li, B. Berkemeier, M. Hull, S. Bhattacharyya, M. Cameron, J. Liu, K. Smith, et al. 2016. Rapid inflammasome activation following mucosal SIV infection of rhesus monkeys. *Cell* 165: 656–667.
46. Unger, B. L., S. Ganesan, A. T. Comstock, A. N. Faris, M. B. Hershenson, and U. S. Sajjan. 2014. Nod-like receptor X-1 is required for rhinovirus-induced barrier dysfunction in airway epithelial cells. *J. Virol.* 88: 3705–3718.
47. Cui, J., Y. Li, L. Zhu, D. Liu, Z. Songyang, H. Y. Wang, and R. F. Wang. 2012. NLRP4 negatively regulates type I interferon signaling by targeting the kinase TBK1 for degradation via the ubiquitin ligase DTX4. *Nat. Immunol.* 13: 387–395.
48. Zhang, L., J. Mo, K. V. Swanson, H. Wen, A. Petrucelli, S. M. Gregory, Z. Zhang, M. Schneider, Y. Jiang, K. A. Fitzgerald, et al. 2014. NLRC3, a member of the NLR family of proteins, is a negative regulator of innate immune signaling induced by the DNA sensor STING. *Immunity* 40: 329–341.
49. Rebsamen, M., J. Vazquez, A. Tardivel, G. Guarda, J. Curran, and J. Tschopp. 2011. NLRX1/NOD5 deficiency does not affect MAVS signalling. *Cell Death Differ.* 18: 1387.
50. Ling, A., F. Soares, D. O. Croitoru, I. Tattoli, L. A. Carneiro, M. Boniotto, S. Benko, D. J. Philpott, and S. E. Girardin. 2012. Post-transcriptional inhibition of luciferase reporter assays by the Nod-like receptor proteins NLRX1 and NLRC3. *J. Biol. Chem.* 287: 28705–28716.
51. Conti, B. J., B. K. Davis, J. Zhang, W. O'connor, Jr., K. L. Williams, and J. P. Ting. 2005. CATERPILLER 16.2 (CLR16.2), a novel NBD/LRR family member that negatively regulates T cell function. *J. Biol. Chem.* 280: 18375–18385.
52. Schneider, M., A. G. Zimmermann, R. A. Roberts, L. Zhang, K. V. Swanson, H. Wen, B. K. Davis, I. C. Allen, E. K. Holl, Z. Ye, et al. 2012. The innate immune sensor NLRC3 attenuates Toll-like receptor signaling via modification of the signaling adaptor TRAF6 and transcription factor NF-κB. *Nat. Immunol.* 13: 823–831.
53. Shaw, A. S., and E. L. Filbert. 2009. Scaffold proteins and immune-cell signalling. *Nat. Rev. Immunol.* 9: 47–56.
54. Gorman, J. A., A. Babich, C. J. Dick, R. A. Schoon, A. Koenig, T. S. Gomez, J. K. Burkhardt, and D. D. Billadeau. 2012. The cytoskeletal adaptor protein IQGAP1 regulates TCR-mediated signaling and filamentous actin dynamics. *J. Immunol.* 188: 6135–6144.
55. Kanwar, N., and J. A. Wilkins. 2011. IQGAP1 involvement in MTOC and granule polarization in NK-cell cytotoxicity. *Eur. J. Immunol.* 41: 2763–2773.
56. Chung, L. K., N. H. Philip, V. A. Schmidt, A. Koller, T. Strowig, R. A. Flavell, I. E. Brodsky, and J. B. Bliska. 2014. IQGAP1 is important for activation of caspase-1 in macrophages and is targeted by *Yersinia* pestis type III effector YopM. *MBio* 5: e01402–e01414.
57. Croy, H. E., C. N. Fuller, J. Giannotti, P. Robinson, A. V. Foley, R. J. Yamulla, S. Cosgriff, B. D. Greaves, R. A. von Kleeck, H. H. An, et al. 2016. The poly(ADP-ribose) polymerase enzyme tankyrase antagonizes activity of the β-catenin destruction complex through ADP-ribosylation of axin and APC2. *J. Biol. Chem.* 291: 12747–12760.
58. Hu, Z., C. Yan, P. Liu, Z. Huang, R. Ma, C. Zhang, R. Wang, Y. Zhang, F. Martinon, D. Miao, et al. 2013. Crystal structure of NLRC4 reveals its autoinhibition mechanism. *Science* 341: 172–175.
59. Maekawa, S., U. Ohto, T. Shibata, K. Miyake, and T. Shimizu. 2016. Crystal structure of NOD2 and its implications in human disease. *Nat. Commun.* 7: 11813.
60. Weissbach, L., J. Settleman, M. F. Kalady, A. J. Snijders, A. E. Murthy, Y. X. Yan, and A. Bernards. 1994. Identification of a human rasGAP-related protein containing calmodulin-binding motifs. *J. Biol. Chem.* 269: 20517–20521.

61. Neel, N. F., J. Sai, A. J. Ham, T. Sobolik-Delmaire, R. L. Mernaugh, and A. Richmond. 2011. IQGAP1 is a novel CXCR2-interacting protein and essential component of the "chemosynapse". *PLoS One* 6: e23813.
62. Uhlén, M., L. Fagerberg, B. M. Hallström, C. Lindskog, P. Oksvold, A. Mardinoglu, Å. Sivertsson, C. Kampf, E. Sjöstedt, A. Asplund, et al. 2015. Proteomics. Tissue-based map of the human proteome. *Science* 347: 1260419.
63. McCall, M. N., H. A. Jaffee, S. J. Zelisko, N. Sinha, G. Hooiveld, R. A. Irizarry, and M. J. Zilliox. 2014. The gene expression barcode 3.0: improved data processing and mining tools. *Nucleic Acids Res.* 42: D938–D943.
64. Harton, J. A., M. W. Linhoff, J. Zhang, and J. P. Ting. 2002. Cutting edge: caterpiller: a large family of mammalian genes containing CARD, pyrin, nucleotide-binding, and leucine-rich repeat domains. *J. Immunol.* 169: 4088–4093.
65. Ye, Z., J. D. Lich, C. B. Moore, J. A. Duncan, K. L. Williams, and J. P. Ting. 2008. ATP binding by monarch-1/NLRP12 is critical for its inhibitory function. *Mol. Cell. Biol.* 28: 1841–1850.
66. Smith, J. M., A. C. Hedman, and D. B. Sacks. 2015. IQGAPs choreograph cellular signaling from the membrane to the nucleus. *Trends Cell Biol.* 25: 171–184.
67. Kufer, T. A., E. Kremmer, D. J. Banks, and D. J. Philpott. 2006. Role for erbin in bacterial activation of Nod2. *Infect. Immun.* 74: 3115–3124.
68. Saitoh, T., N. Fujita, T. Hayashi, K. Takahara, T. Satoh, H. Lee, K. Matsunaga, S. Kageyama, H. Omori, T. Noda, et al. 2009. Atg9a controls dsDNA-driven dynamic translocation of STING and the innate immune response. *Proc. Natl. Acad. Sci. USA* 106: 20842–20846.
69. Crow, Y. J. 2015. Type I interferonopathies: mendelian type I interferon up-regulation. *Curr. Opin. Immunol.* 32: 7–12.
70. Taganov, K. D., M. P. Boldin, K. J. Chang, and D. Baltimore. 2006. NF-kappaB-dependent induction of microRNA miR-146, an inhibitor targeted to signaling proteins of innate immune responses. *Proc. Natl. Acad. Sci. USA* 103: 12481–12486.
71. Baetz, A., M. Frey, K. Heeg, and A. H. Dalpke. 2004. Suppressor of cytokine signaling (SOCS) proteins indirectly regulate toll-like receptor signaling in innate immune cells. *J. Biol. Chem.* 279: 54708–54715.
72. Kayagaki, N., Q. Phung, S. Chan, R. Chaudhari, C. Quan, K. M. O'Rourke, M. Eby, E. Pietras, G. Cheng, J. F. Bazan, et al. 2007. DUBA: a deubiquitinase that regulates type I interferon production. *Science* 318: 1628–1632.
73. Surpris, G., and A. Poltorak. 2016. The expanding regulatory network of STING-mediated signaling. *Curr. Opin. Microbiol.* 32: 144–150.
74. Abel, A. M., K. M. Schuldt, K. Rajasekaran, D. Hwang, M. J. Riese, S. Rao, M. S. Thakar, and S. Malarkannan. 2015. IQGAP1: insights into the function of a molecular puppeteer. *Mol. Immunol.* 65: 336–349.
75. Owen, D., L. J. Campbell, K. Littlefield, K. A. Evetts, Z. Li, D. B. Sacks, P. N. Lowe, and H. R. Mott. 2008. The IQGAP1-Rac1 and IQGAP1-Cdc42 interactions: interfaces differ between the complexes. *J. Biol. Chem.* 283: 1692–1704.
76. Brandt, D. T., S. Marion, G. Griffiths, T. Watanabe, K. Kaibuchi, and R. Grosse. 2007. Dia1 and IQGAP1 interact in cell migration and phagocytic cup formation. *J. Cell Biol.* 178: 193–200.
77. Okada, M., Y. Hozumi, K. Iwazaki, K. Misaki, M. Yanagida, Y. Araki, T. Watanabe, H. Yagisawa, M. K. Topham, K. Kaibuchi, and K. Goto. 2012. DGKζ is involved in LPS-activated phagocytosis through IQGAP1/Rac1 pathway. *Biochem. Biophys. Res. Commun.* 420: 479–484.
78. Kim, H., C. D. White, Z. Li, and D. B. Sacks. 2011. *Salmonella enterica* serotype Typhimurium usurps the scaffold protein IQGAP1 to manipulate Rac1 and MAPK signalling. *Biochem. J.* 440: 309–318.
79. Mukai, K., H. Konno, T. Akiba, T. Uemura, S. Waguri, T. Kobayashi, G. N. Barber, H. Arai, and T. Taguchi. 2016. Activation of STING requires palmitoylation at the Golgi. *Nat. Commun.* 7: 11932.
80. Helgason, E., Q. T. Phung, and E. C. Dueber. 2013. Recent insights into the complexity of Tank-binding kinase 1 signaling networks: the emerging role of cellular localization in the activation and substrate specificity of TBK1. *FEBS Lett.* 587: 1230–1237.
81. Suzuki, T., H. Oshiumi, M. Miyashita, H. H. Aly, M. Matsumoto, and T. Seya. 2013. Cell type-specific subcellular localization of phospho-TBK1 in response to cytoplasmic viral DNA. *PLoS One* 8: e83639.
82. McDonald, C., F. F. Chen, V. Ollendorff, Y. Ogura, S. Marchetto, P. Lécine, J. P. Borg, and G. Nuñez. 2005. A role for Erbin in the regulation of Nod2-dependent NF-kappaB signaling. *J. Biol. Chem.* 280: 40301–40309.
83. Kabi, A., and C. McDonald. 2012. FRMBP2 directs NOD2 to the membrane. *Proc. Natl. Acad. Sci. USA* 109: 21188–21189.
84. Nakamura, N., J. R. Lill, Q. Phung, Z. Jiang, C. Bakalarski, A. de Mazière, J. Klumperman, M. Schlatter, L. Delamarre, and I. Mellman. 2014. Endosomes are specialized platforms for bacterial sensing and NOD2 signalling. *Nature* 509: 240–244.
85. Travassos, L. H., L. A. Carneiro, M. Ramjeet, S. Hussey, Y. G. Kim, J. G. Magalhães, L. Yuan, F. Soares, E. Chea, L. Le Bourhis, et al. 2010. Nod1 and Nod2 direct autophagy by recruiting ATG16L1 to the plasma membrane at the site of bacterial entry. *Nat. Immunol.* 11: 55–62.